Chemotherapy-driven *de novo* Wnt pathway activation dictates a dynamic shift to a drug-tolerant state in breast cancer cells

Youssef El Laithy[1], Willy Antoni Abreu De Oliveira[1], Anirudh Pabba[2], Alessandra Qualizza[1], François Richard[2], Paraskevi Athanasouli[1], Carla Rios Luci[3], Wout De Wispelaere[4], Larissa Mourao[5], Siân Hamer[6], Stijn Moens[4], Anchel De Jaime-Soguero[1], Maria Francesca Baietti[7], Stefan J Hutten[8,9], Jos Jonkers[8,9], Stephen-John Sammut[10,11], Stefaan Soenen[3], Colinda LGJ Scheele[5], Alejandra Bruna[6], Christine Desmedt[2], Daniela Annibali[4], Frederic Lluis[1*].

[1] Stem Cell Institute, Department of Development and Regeneration, Katholieke Universiteit (KU) Leuven, Leuven, 3000, Belgium.
[2] Laboratory for Translational Breast Cancer Research, Department of Oncology, KU Leuven, Leuven, 3000 Belgium.
[3] NanoHealth and Optical Imaging Group, Department of Imaging & Pathology, KU Leuven, Leuven, 3000, Belgium.
[4] Gynecological Oncology, Department of Oncology, KU Leuven, Leuven, 3000, Belgium.
[5] Laboratory of Intravital Microscopy and Dynamics of Tumor Progression, Department of Oncology, VIB-KU Leuven Center for Cancer Biology, Leuven, 3000, Belgium.
[6] Preclinical Modelling of Pediatric Cancer Evolution, Institute of Cancer Research (ICR), London, SM2 5NG, United Kingdom.
[7] TRACE – Laboratory for RNA Cancer Biology, Department of Oncology, KU Leuven, Leuven, 3000 Belgium.
[8] Division of Molecular Pathology, The Netherlands Cancer Institute, Amsterdam, 1066CX, The Netherlands.
[9] Oncode Institute, Amsterdam, 1066CX, The Netherlands.
[10] Breast Cancer Now Toby Robins Research Center, Institute of Cancer Research (ICR), London, SM2 5NG, United Kingdom.
[11] The Royal Marsden Hospital, NHS Foundation Trust, London, SW3 6JJ, United Kingdom.

* Correspondence to: Frederic Lluis – frederic.lluisvinas@kuleuven.be

ABSTRACT

The efficacy of chemotherapy is often hindered by the enrichment of drug-tolerant persister (DTP) cells, which are known to drive therapy resistance. Unraveling and targeting the early events leading to therapy-induced DTP cell-enrichment presents a potential avenue for innovative therapeutic strategies. In this study, we identified the activation of the Wnt/β-catenin signaling pathway as a common mechanism underlying early DTP cell-enrichment in response to different chemotherapeutic agents in Triple-negative breast cancer (TNBC). Live-imaging reveals *de novo* transcriptional Wnt-activation prevailing over intrinsic selection post chemotherapy. Importantly, Wnt-active (Wnt^{High}) cells exhibit transcriptional and functional similarities to DTP cells, such as a diapause transcriptional signature, reduced proliferation, and marked chemoresistance. The transition to a post-treatment Wnt^{High} state is driven by increased expression of key components involved in canonical Wnt ligand-secretion and -activation. Genetic interference or concomitant, rather than sequential, pharmacologic inhibition of Wnt ligand-secretion alongside chemotherapy prevents treatment-induced Wnt^{High} enrichment, sensitizing TNBC tumors to chemotherapy. This study enhances our understanding of the introductory mechanisms driving DTP cell-enrichment upon chemotherapy.

INTRODUCTION

Systemic cytotoxic chemotherapy, employing different drugs such as taxanes, anthracyclines, or platinum-based salts, is one of the most widely accepted treatment modalities for malignant tumors, including triple-negative breast cancer (TNBC)[1–3]. Many patients with TNBC initially benefit from preoperative (neoadjuvant) chemotherapy (NAC); however, about 30%–50% develop resistance, leading to poor overall survival rates[4,5]. Accumulating evidence indicates that cancer cells enter a reversible drug-tolerant persister (DTP) cell-state to evade chemotherapy-induced cell death, leading to incomplete response and/or recurrence[6–8]. DTP cells are characterized by a slow-cycling rate, stem-like traits (including the expression of stem cell- and epithelial-to-mesenchymal (EMT) -markers), and a drug-resistant phenotype[6–8]. One crucial distinction between DTP cells and cancer stem cells (CSCs) is that the DTP cell-state is a rapidly acquired, dynamic, and reversible state – cycling between sensitive and resistant phenotypes[8]. Remarkably, various chemotherapeutic agents, each with distinct mechanisms of action, have demonstrated the ability to mediate the enrichment of DTP cells[9], suggesting the existence of common cellular mechanisms driving drug resistance among diverse therapeutic approaches.

Drug tolerant cell-enrichment and drug resistance have conventionally been attributed to the selection of pre-existing resistant (stem)-cell population(s) (referred to as intrinsic or Darwinian selection)[10]. However, recent research using genomic and transcriptomic deep sequencing of matched longitudinal (pre- and post-NAC treatment) TNBC patient and patient-derived xenograft (PDX) samples have also highlighted the role of acquired (drug-induced) resistance during chemotherapy[11,12]. Here, cancer cells undergo profound transcriptional changes in response to chemotherapeutic aggression, effectively acquiring new transcriptional expression profiles that promote their survival and are believed to constitute a defensive mechanism against treatment pressure. Notably, the enhanced phenotypic plasticity of TNBC enables a rapid and early acquisition of a drug-tolerant state[13,14]. These findings collectively emphasize that therapy is not only a selective force acting on pre-existing resistant cells, but also a driver of signaling cues that lead to cellular transcriptional reprogramming, cell identity switching, and the emergence of DTP cell-populations. Even though recent studies have focused on the genomic, epigenetic, and transcriptomic contributions to TNBC tumor evolution and cell plasticity during treatment[11,15], knowledge concerning the signaling pathways and mechanisms that operate during the early stages of drug tolerant cell(s) emergence in response to chemotherapy remains limited.

The Wnt/β-catenin signaling pathway regulates a variety of cellular processes, including cell fate commitment, differentiation, proliferation, and stem cell maintenance[16,17]. Wnt proteins (Wnts) are a family of 19 secreted, glycosylated, and palmitoylated ligands which primarily interact with Frizzled (FZD) receptors and/or low-density-lipoprotein receptor-related proteins 5/6 (LRP5/6) to promote activation of the canonical (β-catenin-dependent) or non-canonical (β-catenin-independent) pathways[18]. Activation of the canonical Wnt signaling pathway leads to stabilization of β-catenin promoting the transcription of target genes. Wnt signaling is potentiated by the presence of R-spondin (RSPO) ligands, binding Leu-rich repeat-containing G-protein coupled receptor 4-6 (LGR4-6) co-receptors preventing FZD receptor degradation[18].

When dysregulated, Wnt signaling is a driver of tumorigenesis and chemoresistance in several human cancers, including colorectal, liver, gastric cancer or TNBC. Importantly, activation of the canonical Wnt signaling pathway and β-catenin stabilization have been correlated with unfavorable prognosis in patients with TNBC[19–24]. Due to its capacity in regulating cell cycle, lineage commitment, and stem cell maintenance, activation of the canonical Wnt signaling pathway is associated with a pro-proliferative and cancer stem cell state[16,20,21,25]. Current research has predominantly focused on understanding the role of Wnt signaling activation in TNBC tumors under baseline or unchallenged conditions, overlooking the dynamics occurring during chemotherapeutic treatment[24,26,27].

Identifying and subsequently targeting the introductory, non-genetic events responsible for the enrichment of drug-tolerant cell-populations in TNBC could pave the way for novel therapeutic strategies to prevent treatment resistance. First, using TNBC cell lines, we show that *de novo* Wnt transcriptional activation precedes drug-tolerant cell(s) enrichment regardless of the chemotherapeutic agent (docetaxel or carboplatin) used. Activation of the Wnt signaling pathway by cytotoxic treatment was not limited *to in vitro* 2D-cultured TNBC cell lines but was also consistently observed in 3D-cultured TNBC patient-derived organoid (PDO) models as well as *in vivo* xenograft models. Furthermore, analysis of paired (NAC-treated, pre- vs. post-treatment) BC patient datasets, of which patients did not achieve pathological complete response (pCR), also showed differential enrichment of the Wnt signaling pathway. Following transcriptomic and functional analyses of chemotherapy-treated Wnt^{High} cells, we observed a notable correlation between Wnt-activation and the acquisition of DTP cell features. This association was evidenced by a significant transcriptional correlation with an embryonic diapause gene signature, reduced proliferation, and enhanced resistance capacity to chemotherapy. Further analysis revealed that

chemotherapy-induced Wnt-activation is mediated through increased expression and secretion of Wnt ligands and/or Wnt enhancers.

We demonstrate that combinatorial, rather than sequential, treatment involving concomitant pharmacological inhibition of Wnt ligand-secretion alongside chemotherapy hinders chemotherapy-induced Wnt-activation and significantly sensitizes TNBC cell lines, xenograft models, and PDO models to chemotherapy. Our findings suggest that patients undergoing chemotherapy treatment may potentially encounter aberrant activation of the Wnt signaling pathway leading to drug-tolerant cell enrichment. This implies that a combinatorial treatment strategy involving both Wnt ligand secretion-inhibition and chemotherapy might effectively target the initial mechanisms involved in the enrichment and/or acquisition of a DTP cell-phenotype while subsequently providing clinical benefits for patients with TNBC undergoing systemic chemotherapy.

RESULTS

Wnt-transcriptional activation precedes drug-tolerant cell(s) enrichment upon chemotherapeutic treatment

To study the molecular basis of drug-tolerant cell(s) emergence or enrichment during therapy, we recapitulated this phenomenon *in vitro*. MDA-MB-231, MDA-MB-468, and PDC-BRC-101 TNBC cell lines were subjected to two separate chemotherapeutic agents: docetaxel (DOC) and carboplatin (CAR). These agents operate through different mechanisms of action, with DOC promoting microtubule stabilization and preventing depolymerization, and CAR inducing DNA damage[28,29]. IC50 concentrations (at 72h) were determined for each chemotherapeutic agent for every cell line and used in successive studies (Supplementary Fig. S1a-f). To assess changes in the frequency of putative drug-tolerant cells under chemotherapeutic pressure, the enzymatic activity of aldehyde dehydrogenase 1 (ALDH1), a functional stem cell marker in solid tumors whose expression is linked to drug resistance and the DTP cell-phenotype in TNBC[30,31], was assessed. Treatment of all TNBC cell lines with IC50 concentrations of either DOC or CAR led to a significant increase in the levels of $ALDH^+$ cells compared to untreated (UNT) conditions at 96hours(h) but not at 48h (Fig. 1a-c) indicating a time-dependent effect on drug-tolerant cell(s) enrichment following chemotherapeutic treatment.

To gain insights into the signaling cues preceding and, potentially, driving this chemotherapy-mediated enrichment of drug-tolerant ($ALDH^+$) cells at 96h, we performed bulk transcriptomic analysis of mRNA-sequenced samples obtained from viable/drug-tolerant ($DAPI^-$) MDA-MB-231 cells treated with either DOC or CAR at 72h (Supplementary Fig. S1g-i). Gene Set Enrichment Analysis[32] (GSEA) using MSigDB[33] datasets on differentially expressed genes (DEGs – Supplementary Fig. S1h, i, and Supplementary Table 1) between DOC vs. UNT or CAR vs. UNT ($FC > 1.5$, $p\text{-val} \leq 0.05$) identified an array of Hallmarks significantly enriched in DOC or CAR treatments, including Apoptosis, p53 Pathway, and Interferon Gamma Response, which align with the expected cell stress induced by chemotherapeutic exposure (Fig. 1d, Supplementary Fig. S1j, k and Supplementary Table 2)[15]. Conversely, Hallmarks associated with cell cycle regulation were downregulated in DOC and CAR treatments (Fig. 1d) in line with findings of previous reports[15,34]. Interestingly, EMT and Hypoxia, both associated with tumorigenesis and drug-tolerance, were enriched in response to chemotherapeutic exposure (Fig. 1d and Supplementary Fig. S1j, k)[35,36].

To elucidate common transcriptomic alterations among distinct chemotherapeutic agents, we performed Gene Ontology (GO) analysis using the commonly (DOC & CAR vs. UNT) upregulated (1381) genes shared between both drugs (Fig. 1e). GO analysis repeatedly highlighted a significant enrichment of (positive)

regulation of Canonical Wnt signaling, which was corroborated with an enrichment in the expression of Wnt-targets (*AXIN2* and *LGR5*) and upstream regulators and activators (*WLS* and *WNT2B*) of the pathway (Fig. 1f, g). Conversely, GO analysis using commonly downregulated (785) genes shared between both drugs highlighted significant enrichment in processes related to cell cycle regulation and progression (Supplementary Fig. S1l, m).

Western Blot analysis of active (non-phosphorylated) β-catenin in TNBC cell lines confirmed increased levels of active β-catenin, as early as 24 h post-treatment, and prolonged for up to 6 days (Fig. 1h-j). Consequently, the expression levels of Wnt signaling target-genes (*AXIN2* and *LGR5*) showed a significant increase, mirroring the elevated expression of stemness-associated markers (*SOX2*, *POU5F1*, and *NANOG*) (Fig. 1k-m)[37–39].

Our data reveals an upregulation of canonical Wnt signaling activity preceding ALDH-enrichment. Notably, this enrichment or activation of the Wnt signaling pathway appears to be a common phenomenon shared among various TNBC cell lines and in response to two distinct cytotoxic treatments.

Induction of transient *de novo* Wnt signaling transcriptional activation in response to chemotherapy in TNBC cell lines

To gain a more comprehensive understanding and an ability to monitor the kinetics orchestrating chemotherapy-mediated Wnt signaling enrichment at the population level in living cells, we generated clonal MDA-MB-231, MDA-MB-468, and PDC-BRC-101 TNBC cell lines carrying a stable integrated Wnt-transcriptional (β-catenin-TCF/LEF-mediated transcriptional activity) reporter (TOP-GFP/TGP lines)[40] (Fig. 2a). We observed a range of TOP-GFP expression patterns in all three TNBC cell lines cultured in basal conditions, with an approximate 6%, 2.5%, and 10% GFP^+ (referred to hereafter as Wnt^{High}) cells in MDA-MB-231-TGP, MDA-MB-468-TGP, and PDC-BRC-101-TGP cell lines, respectively (Fig. 2a and Supplementary Fig. S2a – top panel). Stimulating transcriptional activation levels of the Wnt signaling pathway with CHIR99021, a small molecule serving as a GSK3β inhibitor, resulted in high levels of GFP-expression – reaching >97% Wnt^{High} cells – confirming the fidelity of the reporter cell lines (Supplementary Fig. S2a – bottom panel and S2b). Upon exposure to either DOC or CAR agents, we observed a significant increase in the percentage of Wnt^{High} cells in viable/drug-tolerant ($DAPI^-$) cells compared to UNT (Fig. 2b-d and Supplementary Fig. S2c). Prolonged exposure to either therapeutic agent for 6 days maintained or increased the percentage of transcriptional Wnt^{High} cells (Fig. 2b-d), confirming that the enrichment and/or induction of Wnt^{High} cells is one of the early events directing drug-tolerance. Intriguingly, we observed that the median fluorescence intensity (MFI) of the GFP recorded in the chemotherapy-treated Wnt^{High}

population was significantly higher than that of the UNT Wnt^{High} population (Supplementary Fig. S2d), suggesting that chemotherapy treatment not only augments the percentage of transcriptionally Wnt-active cells in the drug-tolerant population but also enhances the levels of transcriptional Wnt-activation. While live-cell imaging analysis of MDA-MB-231-TGP and PDC-BRC-101-TGP TNBC cell lines under UNT conditions did not reveal significant changes in the levels of Wnt^{High} cells (Fig. 2e and Supplementary Fig. S2e – black lines), treatment with either DOC or CAR resulted in a gradual enrichment of Wnt^{High} cells over a similar chemo-culture timespan (Fig. 2e and Supplementary Fig. S2e), consistent with our previous FACS-based results.

To visualize Wnt-transcriptional activation dynamics at single-cell resolution, we tracked the original Wnt-state of Wnt^{High} cells (starting at 60h back to 0h) under UNT or chemotherapy-treated conditions. In UNT conditions, 55% of Wnt^{High} cells in the MDA-MB-231-TGP cell line observed at 60h were initially Wnt^{High} at T_0, while 34% were activated during the culture span (mode #2 and #1, respectively) (Fig. 2f, g, Supplementary rep. images Fig. S2f – top panel, and Supplementary Videos SV1, 2). In contrast, under DOC or CAR treatment conditions, the majority of Wnt^{High} cells at 60h (58% and 55%, respectively) were *de novo*-activated during treatment, indicating chemotherapy-induced Wnt-activation in initially Wnt^{Low} cells (GFP^- at T_0 – mode #1). Conversely, only 27% and 34% of Wnt^{High} cells in DOC and CAR treatment conditions were initially Wnt^{High} at T_0 (mode #2) (Fig. 2h, i, rep. images Fig. 2j, k, Supplementary rep. images Fig. S2f – middle and bottom panel, and Supplementary Videos SV3-6). These findings suggest that chemotherapy-induced Wnt pathway-enrichment mainly results from *de novo* activation rather than only passive selection of initially Wnt^{High} cells. Additional modes of Wnt-transcriptional activation dynamics were observed in a minority of cases (mode #3 and #4) while cells that fell out of the imaging frame were considered of unknown origin/state (mode #5). In accordance with these findings, similar observations were validated using the PDC-BRC-101-TGP cell line (Supplementary Fig. S2g-i).

Next, we assessed the population dynamics of chemotherapy-induced Wnt^{High} cells after treatment was halted (Fig. 2l). Interestingly, the percentage of Wnt^{High} cells was stabilized or even increased upon chemotherapy removal for up to 3 weeks (Fig. 2m-p). Prolonged culture of these cells for 4 weeks in chemo-free conditions resulted in a significant reduction in the percentage of Wnt^{High} cells, re-establishing the Wnt-population to levels similar to that of UNT/basal-cultured cells. This data indicates that the chemotherapy-induced Wnt^{High} phenotype is transient and reversible at the population level once treatment pressure is removed (Fig. 2m-p and Supplementary Fig. S2j).

Altogether, these findings show that the Wnt^{High} phenotype results namely from a *de novo* chemotherapy-driven action rather than solely representing a manifestation of an inherently chemotherapy-resistant

subpopulation selected under treatment pressure. Notably, upon chemotherapy removal, Wnt-activity levels revert to baseline levels, indicating a transient Wnt^{High} state dependent on chemotherapy pressure.

Bulk mRNA-sequencing of transcriptionally differential Wnt-populations reveals that chemotherapy-treated Wnt^{High} cells display DTP cell-properties

To unravel the transcriptional discrepancies between the Wnt^{Low} and Wnt^{High} populations, we conducted bulk transcriptomic analysis on mRNA-sequenced samples derived from viable/drug-tolerant ($DAPI^-$) MDA-MB-231-dTGP sorted populations in chemotherapy-treated conditions (Supplementary Fig. S3a)[41]. Gene set variation analysis (GSVA) revealed a plethora of MSigDB Hallmark signatures from DEGs between CAR or DOC (FC > 1.5, p-val ≤ 0.05) in Wnt^{High} vs. Wnt^{Low} sorted cells that were differentially up- or down-regulated (Supplementary Fig. S3b, c, and Supplementary Tables 3-5).

As expected, the Wnt signaling pathway was significantly and positively associated in CAR- and DOC-sorted Wnt^{High} populations compared to Wnt^{Low} populations (Fig. 3a and Supplementary Fig. S3e). While a few signatures exhibited drug-dependent associations, most differentially regulated hallmarks followed a similar associative trend among sorted chemo-treated Wnt^{High} and Wnt^{Low} cells observed across both drug treatments (Fig. 2a-d and Supplementary Fig. S3e). Notably, developmental signaling pathways, including Hedgehog, Notch, IL-6/JAK/STAT3, and TGF-β signaling, along with hallmarks linked to tumor progression, stemness capacity, and metastasis[42–44] (e.g., Angiogenesis and EMT), displayed a significant positive association with Wnt^{High} populations in comparison to Wnt^{Low} populations (Fig. 3a, b, and Supplementary Fig. S3e). Conversely, the TNF-α signaling pathway via the NF-κB pathway notably exhibited a significant negative association with Wnt^{High} cells (Fig. 3a and Supplementary Fig. S3e) aligning with previous findings suggesting that active β-catenin can attenuate transcriptional NF-κB activity in breast cancer[45].

Even though Wnt pathway-activation has been shown to correlate with increased proliferation[46], our transcriptional analysis revealed that Wnt^{High} cells negatively correlated with transcriptional signatures of proliferation, as evidence by significant reduction of a MYC target, G2M checkpoint, and E2F target signatures across chemo-treated Wnt^{High} samples (Fig. 3c and Supplementary Fig. 3e)[19,46]. In addition, a significant negative association was also identified for chemo-treated Wnt^{High} cells and Caspase3/Apoptosis signatures (Fig. 3d and Supplementary Fig. 3e). Notably, the coordinated upregulation of hallmarks associated with Notch and EMT alongside downregulation of MYC targets and Caspase3/Apoptosis signatures observed in Wnt^{High} cells mirrors crucial cellular processes involved in the functionality of DTPs[9,47] suggesting that Wnt^{High} cells may transcriptionally resemble DTP cells (Fig. 3e).

A remarkable recent finding has been the observation that cancer DTP cells and embryonic diapause cells share an extensive transcriptional profile[9,47,48]. Recently, Rehman et al. identified a distinctive embryonic diapause gene signature which significantly correlated with cancer DTP cells. Interestingly, we observed a significant positive association between the diapause/DTP gene signature and sorted chemo-treated Wnt^{High} cells, further providing evidence regarding Wnt^{High} cells resembling a transcriptional DTP cell-state (Fig. 3f).

We aimed to explore if the observed transcriptional changes in Wnt^{High} cells under chemotherapy pressure were already pre-existing in UNT conditions. Despite a positive correlation between Wnt^{High} cells obtained from UNT conditions and the Wnt/β-catenin hallmark signature, the association was not statistically significant (Fig. 3a), consistent with our previous data highlighting lower levels of Wnt signaling-activity/intensity in UNT samples (Supplementary Fig. S2d). Interestingly, UNT-derived Wnt^{High} cells exhibited overall positive associations with developmental signaling pathways and significant positive associations with EMT, while exhibiting significant negative associations with cell cycle hallmarks, including MYC targets (Fig. 3a-d and Supplementary Fig. S3e). Moreover, unchallenged Wnt^{High} cells displayed a notable correlation with the diapause/DTP gene signature (Fig. 3e, f), highlighting transcriptional Wnt-activity as a functional marker for early DTP cells. The significance of this correlation becomes more apparent in chemo-treated conditions, where transcriptional Wnt-activation is strongly exacerbated.

Functional analyses confirmed reduced cell proliferation measured by cell number (Fig. 3g) observed in chemo-sorted Wnt^{High} compared to Wnt^{Low} populations (Fig. 3h). Furthermore, co-staining of GFP-expression (reporter for Wnt-activity) alongside the apoptotic marker Annexin V revealed that Wnt^{High} cells displayed reduced apoptotic activity confirming their enhanced drug-tolerant state (Fig. 3i).

In summary, our comprehensive data reveals that chemotherapy-treated Wnt^{High} cells share a transcriptional profile with cancer DTP cells including a recently identified diapause/DTP gene signature. Functional assessments further confirm a drug-tolerant state strongly pronounced in chemotherapy-enriched Wnt^{High} cells suggesting that transcriptional Wnt-activity might serve as a functional indicator of early drug-tolerance, especially following chemotherapeutic challenge.

Chemotherapeutic treatment induces elevated transcriptional expression of Wnt ligands, Wnt enhancers, and Wnt secretion machinery components

The Wnt signaling pathway is highly conserved and activated via the binding of (19) extracellular Wnt ligands (Wnts) to membrane receptors[19]. Secretion of Wnt ligands requires the action of the

acyltransferase Porcupine (PORCN) followed by Wntless/evenness interrupted (WLS/Evi) which supports transport of Wnts from the Trans-Golgi Network to the plasma membrane. In addition, the Rspo protein family has been shown to enhance Wnt ligand activity to further promote Wnt pathway-activation[18,19].

RT-qPCR screening, focusing on established canonical Wnt ligands (Wnt-1, Wnt-2, Wnt-2b, Wnt-3, Wnt-3a, and Wnt-7b), Wnt ligand enhancers/amplifiers (Rspo1-4), and Wnt secretion machinery components (WLS/Evi and PORCN), revealed that the transcriptional expression of key genes, including *WNT2B*, *WNT3*, *WNT3A*, *WNT7B*, *RSPO1*, *RSPO3*, *WLS*, and *PORCN* was found to be steadily expressed in basal conditions across all analyzed TNBC cell lines (Supplementary Fig. S4a-c).

Importantly, these genes exhibited a consistent and statistically significant increase in expression levels under chemotherapy-treatment conditions (Fig. 4a-c) suggesting that chemotherapeutic exposure actively promotes elevated transcription levels of several key components involved in canonical Wnt pathway-activation.

Subsequently, following chemotherapy removal and under one week chemo-recovery conditions, the majority of Wnt-activation components maintained elevated expression levels (Fig. 4d, e – pink bars) However, after four weeks of culture in chemo-free conditions and coinciding with the previous results displaying the return of Wnt^{High} cells to basal levels (Fig. 2m-p), we observed a corresponding decrease in expression level patterns of Wnt-activation components (Fig. 4d, e – light blue bars). This correlation between the expression levels of Wnt-activation components and the dynamic induction of a Wnt^{High} population highlights the transient nature of chemotherapy-induced Wnt-activation (Fig. 2m-p), providing a possible mechanism for the enrichment of a Wnt^{High} population in response to treatment.

Western blot analysis confirmed the upregulation of the Wnt ligand Wnt-2b and the acyltransferase PORCN, in response to either DOC or CAR treatments across all analyzed TNBC cell lines (Fig. 4f-k).

Treatment of chemo-naïve cells with concentrated conditioned media (CM) derived from MDA-MB-231 and MDA-MB-468 TNBC cell lines (Fig. 4l) confirmed increased and functional presence of Wnt ligands in media collected under one week chemo-recovery conditions, resulting in a significant increase in Wnt^{High} cells when compared to chemo-naïve cells treated with UNT CM (Fig. 4m, n). In a parallel experiment, we co-cultured chemo-naïve (MDA-MB-231-mCherry-TGP) cells with chemo-recovering (MDA-MB-231) cells (Fig. 4o). This co-culturing approach similarly resulted in a substantial and statistically significant increase in the percentage of Wnt^{High} cells within the chemo-naïve cell population (Fig. 4p).

In summary, our findings demonstrate that chemotherapeutic treatment leads to elevated expression levels of Wnt ligands, -enhancers, and -components of the Wnt secretory apparatus. Significantly,

concentrated CM obtained from chemo-treated and recovered cells induces an enrichment in the Wnt^{High} cell population, substantiating the functional impact of the chemo-secreted factors.

Concomitant inhibition of Wnt ligand secretion enhances chemotherapeutic sensitivity in TNBC cell lines

We stably transduced MDA-MB-231, MBD-MB-468, and PDC-BRC-101 TNBC cell lines with lentiviral shRNA constructs designed to silence the acetyltransferase PORCN, avoiding the O-palmitoylation and functional secretion of Wnt ligands[49,50]. The silencing of PORCN led to a substantial reduction (approx. 80-90%) in PORCN mRNA levels (Supplementary Fig. S5a-c). PORCN silenced (shPORCN#1) cell lines exposed to either chemotherapeutic agent revealed reduced levels of active β-catenin or percentage of Wnt^{High} cells compared to control (shPLKO) lines, confirming an essential role for PORCN in chemotherapy-induced Wnt-activation (Fig. 5a-c and Supplementary Fig. S5d). While the silencing of PORCN had no impact on cell viability in basal (UNT) culture conditions, we observed a marked and significant increase in levels of apoptotic (Annexin V^+ and $DAPI^+$) cells in shPORCN#1 TNBC cell lines compared to shPLKO lines, indicating a strong sensitization role of PORCN-inhibition (Fig. 5d-f). We validated the reduction of the chemotherapy-induced Wnt^{High} population and increased sensitization to chemotherapy using a second independent lentiviral shRNA construct targeting PORCN (Supplementary Fig. S5e-g) confirming that genetic inhibition of Wnt ligand secretion effectively hinders the advent of a chemotherapy-induced Wnt^{High} population while significantly enhancing the sensitization of TNBC cell lines to chemotherapy.

In recent years, several pharmacological inhibitors of the acyltransferase PORCN, which effectively abolish the secretion of Wnt ligands, have been developed. These PORCN inhibitors have demonstrated their efficacy in inhibiting Wnt signaling in various solid tumors, including Wnt-deregulated colon cancer and various TNBC cell lines or murine models in baseline conditions[51,52]. Given our previous findings that the Wnt signaling pathway is activated in response to chemotherapeutic treatment, we sought to investigate whether pharmacological inhibition of PORCN could also prove effective in curbing Wnt-activation induced under treatment pressure. We conducted two distinct experimental setups to further investigate this matter. In the first setup, we pre-treated MDA-MB-231, MBD-MB-468, and PDC-BRC-101 TNBC cell lines with the Inhibitor of Wnt Production (IWP-2) for 48h followed by the application of either DOC or CAR agents (Sequential Treatment)[53]. In the second setup, we applied chemotherapeutic treatment simultaneously and in combination with IWP-2 (Combinatorial Treatment).

Pre-treatment (sequential treatment strategy – Fig. 5g) of MDA-MB-231, MBD-MB-468, and PDC-BRC-101 TNBC cell lines with IWP-2 for 48h led to a notable and significant reduction in the percentage of Wnt^{High}

cells as well as a reduction in stem cell marker expression (Fig. 5h, j) with no effects on cell viability (Supplementary Fig. S5h). However, upon chemotherapy addition, we observed robust chemotherapy-induced Wnt-activation and increased stem cell marker expression in IWP-2 pre-treatment conditions when compared to sole chemo-treatment in all TNBC cell lines (Fig. 5i, j). Notably, pre-treatment with IWP-2 followed by chemotherapy addition did not result in increased cell death nor sensitization to either agent (Supplementary Fig. S5i-k), suggesting that a strategy to target *a priori* existent Wnt^{High} population might not be sufficient to prevent chemotherapy-induced Wnt-activation and its subsequent implications.

In the second setup (combinatorial treatment strategy – Fig. 5k), simultaneous treatment of TNBC cell lines with either DOC or CAR therapeutic agent in combination with IWP-2 led to a significant decrease in the percentage of Wnt^{High} cells (Fig. 5l) and a strong reduction in stem cell marker expression (Fig. 5m). This underscores the critical role of Wnt ligand secretion in this acquired Wnt-activation phenomenon. Intriguingly, combinatorial treatment involving chemotherapeutic agents alongside IWP-2 resulted in a substantial increase in apoptotic cell death across all analyzed TNBC cell lines compared to treatment with either chemotherapeutic agent alone (Fig. 5n). Interestingly, we observed that the supplementation of IWP-2 alongside chemotherapy resulted in significant downregulation of drug-tolerant associated genes, *SURVIVIN* and *ABCB1* (Supplementary Fig. S5l)[54,55]. Furthermore, using a second pharmacological PORCN inhibitor, WNT-974 (LGK-974, currently tested in phase I/II clinical trials)[56,57] resulted in similar results obtained with Wnt ligand secretion-inhibitor IWP-2 (Supplementary Fig. 5m-r).

In summary, our findings collectively demonstrate the essential role of Wnt ligand secretion in driving chemotherapy-induced Wnt-activation and chemoresistance. Notably, simultaneous, rather than sequential, treatment with chemotherapeutic agents and pharmacological Wnt ligand secretion-inhibition can significantly curb chemotherapy-induced Wnt-activation and ultimately sensitize TNBC cell lines to chemotherapy.

Inhibition of Wnt ligand secretion and chemotherapeutic treatment synergistically sensitize *in vivo* xenograft TNBC model to treatment

A precise and complete understanding of Wnt-activation kinetics and dynamics in response to chemotherapeutic treatment in *in vivo* models is lacking. To shed some light on this phenomenon, we engineered the TNBC cell line MDA-MB-231 with the Wnt-transcriptional reporter TOPFLASH, a β-catenin-responsive firefly luciferase reporter plasmid compatible for use with the *in vivo* live imaging system (IVIS) (Fig. 6a)[40].

Treatment with either DOC or CAR[58,59] resulted in a significant overall decrease in tumor volume when compared to the vehicle (VEH) treated group (Fig. 6b, c). Notably, at the administered doses, no significant changes in mouse body weight were observed during the three weeks of treatment (Supplementary Fig. S6a). We observed, as early as 48h and 72h (for DOC and CAR, respectively) upon chemotherapeutic administration, a significant upregulation in transcriptional Wnt-activation recorded by IVIS (Fig. 6d, e and representative image Supplementary Fig. S6b). Notably, this activation started to decrease as the week progressed following the 1st dose-administration and again increased significantly 48h and 72h (for DOC and CAR, respectively) following administration of the 2nd and 3rd dose (Fig. 6d, e) highlighting the dynamic behavior of chemotherapy-induced Wnt-activation *in vivo*. Gene expression analysis on the resected tumors following the 3rd and final cycle of chemotherapeutic administration revealed elevated expression of Wnt-targets (*AXIN2* and *LEF1*), stemness markers (*POU5F1* and *SOX2*), Wnt ligands and -enhancers (*WNT2B*, *WNT3A*, *WNT7B*, *RSPO1*, and *RSPO3*), and Wnt secretion machinery components (*WLS* and *PORCN*) (Fig. 6f and Supplementary Fig. S6c, d) in chemotherapy-treated groups.

We next proceeded to assess whether a combinatorial treatment strategy encompassing the use of chemotherapy with a pharmacological Wnt ligand secretion-inhibitor (Fig. 6g) could abrogate Wnt-activation and lead to tumor sensitization, as indicated in our previous *in vitro* findings. Administration of LGK-974 alone had no discernible effect on tumor growth (Fig. 6h, i, and Supplementary Fig. S6e)[60,61]. Conversely, the combination of LGK-974 with either DOC or CAR treatment resulted in a substantial and significant decrease in Wnt pathway-activation, correlating with a marked reduction in tumor volume compared to solo chemo-treated or VEH-groups (Fig. 6h-k and Supplementary Fig. S6e). Notably, LGK-treatment, sole or in combination with either chemotherapeutic agent, had no significant effect on mouse body weight observed during the three weeks of treatment (Supplementary Fig. S6f).

Response Evaluation Criteria in Solid Tumors (RECIST) analysis was performed to assess tumor response to treatment, categorizing objective outcomes into progressive disease (PD), stable disease (SD), partial response (PR), and complete response (CR). In the VEH-group, 75% (6/8) of tumors were classified as PD, and 25% (2/8) were classified as SD (Fig. 6l). Sole LGK-974 treatment showed no difference in RECIST classifications (75% PD and 25% SD) compared to VEH-conditions, indicating minimal impact on tumor burden (Fig. 6l). In solo DOC- or CAR-treated groups, RECIST analysis classified 100% of tumors as SD, demonstrating the efficacy of DOC or CAR treatments in controlling tumor growth (Fig. 6l). In the DOC+LGK treatment arm, LGK-974 supplementation significantly improved objective response with tumors classified as 28.6% SD (2/7) and 71.4% PR (5/7) (Fig. 6l), compared to sole DOC-treatment (100% SD). Similarly, in

the CAR+LGK treatment arm, tumors were classified as 42.8% SD (3/7), 28.6% PR (2/7), and 28.6% CR (2/7), highlighting the positive impact of combining chemotherapy with Wnt secretion-inhibition (Fig. 6l).

Our study comprehensively characterizes the dynamics of the Wnt signaling pathway in chemotherapy-treated tumors within an *in vivo* setting. Furthermore, we demonstrate that a treatment regimen combining chemotherapy and Wnt ligand secretion-inhibition significantly diminishes the enrichment of Wnt pathway-activation and curbs tumor growth.

Preclinical PDO models recapitulate chemotherapy-mediated Wnt-activation and sensitization to synergistic Wnt ligand secretion inhibition

To investigate whether Wnt/β-catenin signaling is enriched in breast cancer patients following exposure to chemotherapy, we conducted transcriptomic analysis on two patient-derived DNA microarray datasets containing paired (pre- and post-NAC treated) samples that did not achieve pCR (GSE87455 and GSE21974 – Supplementary Fig. S7a, b)[62–64](Supplementary Tables 6, 7). Hallmarks and KEGG gene sets from the human MSigDB database consistently identified the Wnt signaling pathway as significantly enriched in tumor samples obtained from patients post-NAC treatment (Supplementary Fig. S7c-f) in both datasets.

We next investigated the effect of chemotherapeutic treatment and Wnt ligand secretion-inhibition on pre-clinical 3D Patient Derived Organoid (PDO) models[65,66]. Two different PDO models, R1-IDC113 (113 BCO) and R2-IDC159A (159A BCO) (Fig. 7a and Supplementary Fig. S7g) were used. Typically, organoid models are cultured in growth factor-dense medium[67], including Wnt ligand (Wnt-3a) and Wnt ligand-enhancer (R-spondin3), possibly influencing studies of Wnt signaling pathway dynamics. Culturing of either cancer organoid model for four passages in a $Wnt^-/Rspo^-$ breast cancer organoid (BCO) medium, had no effects on the morphology, proliferation rate, or viability of either PDO model when compared to a baseline ($Wnt^+/Rspo^+$) BCO medium (Supplementary Fig. S7h, i).

Upon exposure to IC50 concentrations of either DOC or CAR agents in a $Wnt^-/Rspo^-$ BCO media (Supplementary Fig. S7j-m), both PDO models exhibited a substantial and statistically significant increase in the expression levels of Wnt-target genes and stem cell markers, compared to UNT conditions (Fig. 7b, c). Immunofluorescence analysis of active β-catenin levels confirmed increased Wnt-activation in both PDO models following exposure to either chemotherapeutic agent (Fig. 7d and Supplementary Fig. S7n). Additionally, our data confirmed significant elevation in the expression levels of Wnt ligands, -enhancers, and -secretion machinery components in chemotherapy-treated PDO models when compared to UNT

conditions (Fig. 7e, f). Collectively, these results support the notion of robust Wnt signaling pathway-activation in response to chemotherapeutic treatment in two distinct TNBC pre-clinical PDO models.

To investigate the efficacy of the combinatorial treatment strategy, both PDO models were exposed to Wnt ligand secretion-inhibition alone and in combination with escalating concentrations of either chemotherapeutic agent for 96h. Treatment of both PDO models with IWP-2 alone for 96h did not have any effect on cell viability or proliferation (Supplementary Fig. S7o). However, the exposure of both PDO models to chemotherapy in conjunction with IWP-2 demonstrated a significant reduction in the percentage of viable cells compared to chemotherapeutic treatment alone (Fig. 7g-j). Interestingly, this sensitization effect was most effective when IWP-2 was supplemented with sublethal concentrations of chemotherapy (<16nM DOC and <50µM CAR, 113 BCO | <8nM DOC and <125µM CAR, 159A BCO).

In summary, our study demonstrates chemotherapy-induced Wnt-activation in TNBC pre-clinical models and in post-NAC patient derived transcriptomic datasets. Notably, TNBC PDO models exhibited a robust and enhanced sensitization to the combinatorial treatment comprising Wnt ligand secretion-inhibition alongside sub-lethal chemotherapy (<determined IC50) concentrations. This finding underscores the potential clinical significance of this combinatorial approach for breast cancer treatment.

DISCUSSION

The emergence of DTP cells during cancer treatment has become a focal point of oncological research, due to their pivotal role in drug resistance and tumor relapse. Our study delves into an early mechanism, delineating processes of therapy-driven evolution in cancer cells and the enrichment of drug-tolerant cells in response to treatment pressure in TNBC. Our findings reveal a significant enrichment in the percentage of a Wnt^{High} population alongside an increase in the intensity of Wnt-activation in various TNBC models subjected to distinct chemotherapeutic agents. Activation of the Wnt/β-catenin signaling pathway has been linked with CSC renewal and maintenance[19–21,25]. However, in contrast, we establish a significant transcriptional association between the Wnt^{High} population and DTP cells, including a unique diapause/DTP gene signature and a reduction of MYC targets hallmark; both recently correlated with cancer DTP cells[9,47]. Functional analyses confirmed that Wnt^{High} cells exhibit DTP cell-traits such as reduced proliferation and an enhanced capacity for drug tolerance[7,8] Furthermore, the dynamic, transient, and reversible behavior places chemotherapy-treated Wnt^{High} cells closer to the DTP cell criteria and apart from criteria of CSCs, providing a novel perspective for the poor clinical outcomes in TNBC patients with Wnt-deregulation[20,24,26]. This suggests that the transcriptional activation of the Wnt signaling pathway could serve as a distinctive marker for the early emergence of the DTP cell-phenotype, particularly in response to chemotherapeutic exposure.

Current clinical trials investigating PORCN inhibition in TNBC involve the use of a Wnt ligand-inhibitor as monotherapy or in combination with PDR001 (an anti-PD1 antibody), restricted to Wnt-deregulated cancers and excluding consideration of chemotherapy (NCT03447470 and NCT01351103)[56,57]. Our results suggest that combinatorial treatment involving Wnt ligand secretion-inhibition supplemented alongside chemotherapy sensitizes tumors to treatment and holds significant promise for future clinical trials in TNBC. Our study also underscores the importance of temporal considerations in treatment regimens. Crucially, we show that pre-treatment with PORCN inhibitors does not prevent a substantial increase in Wnt^{High} cells or stem cell marker expression once chemo-treatment is applied, indicating that patients undergoing chemotherapy might not benefit from initial treatment with Wnt-inhibitors. Therefore, our findings suggest that simultaneous treatment, rather than sequential treatment, with Wnt-inhibitors and chemotherapy might provide a solution to effectively control chemotherapy-induced drug tolerant cell-enrichment while simultaneously sensitizing tumors to the effects of chemotherapy.

Live-cell imaging, allowing the possibility to track and trace Wnt-reporter TNBC cell lines, revealed that, in contrast to unchallenged (UNT) culture conditions, chemotherapy-mediated enrichment of Wnt^{High} cells is

primarily observed in cells initially in a Wnt^{Low} state, indicating *de novo* activation of the pathway in response to chemotherapeutic treatment. Furthermore, we noted a significant percentage of Wnt^{High} cells in chemo-treated conditions that were initially in a transcriptionally Wnt-active state, suggesting that intrinsic and acquired resistance mechanisms driven by Wnt-transcriptional activity are not mutually exclusive and likely occur simultaneously.

The molecular mechanisms triggering the initial increased expression of Wnt ligands and Wnt enhancers described in this article, or the transcriptional reprogramming previously described in other works in chemotherapy-treated conditions, remain largely unknown[11,12]. Studies in other contexts, such as ovarian cancer, have suggested that chemotherapy-induced stress may induce significant epigenetic changes, indicating a potential role of epigenetic regulation in chemotherapy-induced Wnt pathway-activation[68,69]. Recent research shows that depletion of H3K27me3 (trimethylation of histone H3 at lysine 27) promotes a drug-tolerant state in TNBC and highlights epigenetic regulation as an early event involved in promoting chemoresistance[15]. In our RNA-seq analysis of MDA-MD-231 cells treated with DOC or CAR, we observed around 2,500 upregulated expressed genes (DEGs) 72h post-treatment. Notably, more than 50% (1,650) of these DEGs were common between DOC and CAR treatments, suggesting that the onset of transcriptional reprogramming observed following treatment may be orchestrated by shared molecular mechanisms, even when distinct drugs are used. One possibility is that cells exposed to stress posed by chemotherapeutic pressure may activate pro-survival mechanisms and signaling cues. Interestingly, in regenerative models like *Hydra*, an increase in Wnt ligand expression has been observed in cells undergoing apoptosis as a regenerative pro-survival response to tissue damage[70]. In this article, we propose a mechanistic model for acquired chemoresistance mediated via drug-tolerant cell(s) enrichment in TNBC, comprising two distinct phases. Initially, cells sense environmental changes induced by chemotherapeutic pressure, resulting in increased levels of Wnt ligand(s) and Wnt enhancer(s) transcripts, accompanied by heightened Wnt ligand secretion. Subsequently, to adapt to these environmental pressures, cells transcriptionally activate the Wnt signaling pathway, ultimately giving rise to a defensive and chemotherapy-resistant Wnt^{High} phenotype.

In a recent study by Wang et al., a cell-autonomous mechanism was unveiled, shedding light on how genotoxic treatment in breast cancer cells can activate the Wnt/β-catenin signaling pathway[71]. This activation was mediated through OTULIN, a linear linkage-specific deubiquitinase, which exerted its stabilizing influence on β-catenin through non-Wnt ligand-specific mechanisms. Notably, the OTULIN-dependent stabilization of β-catenin, as detailed in Wang et al.'s work, manifested primarily during the

initial phases of drug treatment, with effects discernible for a maximum of 24h post-chemotherapy exposure. Our current study, in contrast, introduces a novel perspective on chemotherapy-induced Wnt pathway-activation, elucidating a mechanism reliant on Wnt ligands in diverse human TNBC cellular models. Furthermore, our research reveals a sustained and prolonged incidence of chemotherapy-induced Wnt pathway activation that extends well beyond the initial 24h window following treatment initiation. We complement these observations with a comprehensive transcriptional and functional characterization of the Wnt^{High} and Wnt^{Low} populations that emerge as a consequence of chemotherapeutic treatment. Collectively, our findings underscore a previously unrecognized mechanism governing chemotherapy-induced Wnt pathway-activation, emphasizing the vital role of Wnt ligands in this process. To further expand our understanding, future investigations should explore whether ionizing radiation, similar to chemotherapy, can also induce Wnt pathway-activation and whether this occurs via Wnt ligand-dependent or independent mechanisms.

In summary, our research suggests that the secretion of Wnt ligands could play a pivotal role as an early event enhancing the enrichment of DTP cell populations in TNBC and contribute to the development of therapeutic resistance, particularly in response to chemotherapy. Therefore, a potential strategy to address this challenge could involve targeting Wnt ligand-secretion successively hindering chemotherapy-induced Wnt/β-Catenin pathway activation and subsequently diminishing the sustenance and enrichment of DTP cell populations (Fig. 7k).

REFERENCES

1. Bianchini, G., De Angelis, C., Licata, L. & Gianni, L. Treatment landscape of triple-negative breast cancer — expanded options, evolving needs. *Nat. Rev. Clin. Oncol.* **19**, 91–113 (2022).
2. Waks, A. G. & Winer, E. P. Breast Cancer Treatment. *JAMA* **321**, 288 (2019).
3. Nolan, E., Lindeman, G. J. & Visvader, J. E. Deciphering breast cancer: from biology to the clinic. *Cell* **186**, 1708–1728 (2023).
4. Foulkes, W. D., Smith, I. E. & Reis-Filho, J. S. Triple-Negative Breast Cancer. *N. Engl. J. Med.* **363**, 1938–1948 (2010).
5. Liedtke, C. *et al.* Response to Neoadjuvant Therapy and Long-Term Survival in Patients With Triple-Negative Breast Cancer. *J. Clin. Oncol.* **26**, 1275–1281 (2008).
6. Shi, Z.-D. *et al.* Tumor cell plasticity in targeted therapy-induced resistance: mechanisms and new strategies. *Signal Transduct. Target. Ther.* **8**, 113 (2023).
7. Pu, Y. *et al.* Drug-tolerant persister cells in cancer: the cutting edges and future directions. *Nat. Rev. Clin. Oncol.* **20**, 799–813 (2023).
8. Zhang, Z., Tan, Y., Huang, C. & Wei, X. Redox signaling in drug-tolerant persister cells as an emerging therapeutic target. *eBioMedicine* **89**, 104483 (2023).
9. Rehman, S. K. *et al.* Colorectal Cancer Cells Enter a Diapause-like DTP State to Survive Chemotherapy. *Cell* **184**, 226-242.e21 (2021).
10. Marusyk, A., Janiszewska, M. & Polyak, K. Intratumor Heterogeneity: The Rosetta Stone of Therapy Resistance. *Cancer Cell* **37**, 471–484 (2020).
11. Kim, C. *et al.* Chemoresistance Evolution in Triple-Negative Breast Cancer Delineated by Single-Cell Sequencing. *Cell* **173**, 879-893.e13 (2018).
12. Echeverria, G. V. *et al.* Resistance to neoadjuvant chemotherapy in triple-negative breast cancer mediated by a reversible drug-tolerant state. *Sci. Transl. Med.* **11**, (2019).
13. Zawistowski, J. S. *et al.* Enhancer Remodeling during Adaptive Bypass to MEK Inhibition Is Attenuated by Pharmacologic Targeting of the P-TEFb Complex. *Cancer Discov.* **7**, 302–321 (2017).
14. Risom, T. *et al.* Differentiation-state plasticity is a targetable resistance mechanism in basal-like breast cancer. *Nat. Commun.* **9**, 3815 (2018).
15. Marsolier, J. *et al.* H3K27me3 conditions chemotolerance in triple-negative breast cancer. *Nat. Genet.* **54**, 459–468 (2022).
16. Liu, J. *et al.* Wnt/β-catenin signalling: function, biological mechanisms, and therapeutic opportunities. *Signal Transduct. Target. Ther.* **7**, 3 (2022).
17. Yang, K. *et al.* The evolving roles of canonical WNT signaling in stem cells and tumorigenesis: implications in targeted cancer therapies. *Lab. Investig.* **96**, 116–136 (2016).
18. Niehrs, C. The complex world of WNT receptor signalling. *Nat. Rev. Mol. Cell Biol.* **13**, 767–779 (2012).
19. Xu, X., Zhang, M., Xu, F. & Jiang, S. Wnt signaling in breast cancer: biological mechanisms, challenges and opportunities. *Mol. Cancer* **19**, 165 (2020).
20. Pohl, S.-G. *et al.* Wnt signaling in triple-negative breast cancer. *Oncogenesis* **6**, e310–e310 (2017).
21. Abreu de Oliveira, W. A., El Laithy, Y., Bruna, A., Annibali, D. & Lluis, F. Wnt Signaling in the Breast: From Development to Disease. *Front. Cell Dev. Biol.* **10**, (2022).
22. Geyer, F. C. *et al.* β-Catenin pathway activation in breast cancer is associated with triple-negative phenotype but not with CTNNB1 mutation. *Mod. Pathol.* **24**, 209–231 (2011).
23. Zhan, T., Rindtorff, N. & Boutros, M. Wnt signaling in cancer. *Oncogene* **36**, 1461–1473 (2017).
24. Khramtsov, A. I. *et al.* Wnt/β-Catenin Pathway Activation Is Enriched in Basal-Like Breast Cancers and Predicts Poor Outcome. *Am. J. Pathol.* **176**, 2911–2920 (2010).

25. Zheng, H. *et al.* Targeted activation of ferroptosis in colorectal cancer via LGR4 targeting overcomes acquired drug resistance. *Nat. Cancer* (2024) doi:10.1038/s43018-023-00715-8.
26. Geyer, F. C. *et al.* β-Catenin pathway activation in breast cancer is associated with triple-negative phenotype but not with CTNNB1 mutation. *Mod. Pathol.* **24**, 209–231 (2011).
27. Dey, N. *et al.* Wnt signaling in triple negative breast cancer is associated with metastasis. *BMC Cancer* **13**, 537 (2013).
28. Rottenberg, S., Disler, C. & Perego, P. The rediscovery of platinum-based cancer therapy. *Nat. Rev. Cancer* **21**, 37–50 (2021).
29. Verweij, J., Clavel, M. & Chevalier, B. Paclitaxel (TaxolTM) and docetaxel (TaxotereTM): Not simply two of a kind. *Ann. Oncol.* **5**, 495–505 (1994).
30. Dhanyamraju, P. K., Schell, T. D., Amin, S. & Robertson, G. P. Drug-Tolerant Persister Cells in Cancer Therapy Resistance. *Cancer Res.* **82**, 2503–2514 (2022).
31. Raha, D. *et al.* The Cancer Stem Cell Marker Aldehyde Dehydrogenase Is Required to Maintain a Drug-Tolerant Tumor Cell Subpopulation. *Cancer Res.* **74**, 3579–3590 (2014).
32. Subramanian, A. *et al.* Gene set enrichment analysis: A knowledge-based approach for interpreting genome-wide expression profiles. *Proc. Natl. Acad. Sci.* **102**, 15545–15550 (2005).
33. Liberzon, A. *et al.* The Molecular Signatures Database Hallmark Gene Set Collection. *Cell Syst.* **1**, 417–425 (2015).
34. Yadav, N. *et al.* Oxidative phosphorylation-dependent regulation of cancer cell apoptosis in response to anticancer agents. *Cell Death Dis.* **6**, e1969–e1969 (2015).
35. Creighton, C. J. *et al.* Residual breast cancers after conventional therapy display mesenchymal as well as tumor-initiating features. *Proc. Natl. Acad. Sci.* **106**, 13820–13825 (2009).
36. Jing, X. *et al.* Role of hypoxia in cancer therapy by regulating the tumor microenvironment. *Mol. Cancer* **18**, 157 (2019).
37. Jeter, C. R. *et al.* NANOG promotes cancer stem cell characteristics and prostate cancer resistance to androgen deprivation. *Oncogene* **30**, 3833–3845 (2011).
38. Kumar, S. M. *et al.* Acquired cancer stem cell phenotypes through Oct4-mediated dedifferentiation. *Oncogene* **31**, 4898–4911 (2012).
39. Leis, O. *et al.* Sox2 expression in breast tumours and activation in breast cancer stem cells. *Oncogene* **31**, 1354–1365 (2012).
40. Fuerer, C. & Nusse, R. Lentiviral Vectors to Probe and Manipulate the Wnt Signaling Pathway. *PLoS One* **5**, e9370 (2010).
41. Horst, D. *et al.* Differential WNT Activity in Colorectal Cancer Confers Limited Tumorigenic Potential and Is Regulated by MAPK Signaling. *Cancer Res.* **72**, 1547–1556 (2012).
42. Takebe, N. *et al.* Targeting Notch, Hedgehog, and Wnt pathways in cancer stem cells: clinical update. *Nat. Rev. Clin. Oncol.* **12**, 445–464 (2015).
43. Jin, W. Role of JAK/STAT3 Signaling in the Regulation of Metastasis, the Transition of Cancer Stem Cells, and Chemoresistance of Cancer by Epithelial–Mesenchymal Transition. *Cells* **9**, 217 (2020).
44. Liu, S., Ren, J. & ten Dijke, P. Targeting TGFβ signal transduction for cancer therapy. *Signal Transduct. Target. Ther.* **6**, 8 (2021).
45. Ma, B. & Hottiger, M. O. Crosstalk between Wnt/β-Catenin and NF-κB Signaling Pathway during Inflammation. *Front. Immunol.* **7**, (2016).
46. Niehrs, C. & Acebron, S. P. Mitotic and mitogenic Wnt signalling. *EMBO J.* **31**, 2705–2713 (2012).
47. Dhimolea, E. *et al.* An Embryonic Diapause-like Adaptation with Suppressed Myc Activity Enables Tumor Treatment Persistence. *Cancer Cell* **39**, 240-256.e11 (2021).
48. Ramponi, V. *et al.* Persister cancer cells are characterized by H4K20me3 heterochromatin that defines a low inflammatory profile. *bioRxiv* (2024) doi:10.1101/2024.01.26.577389.
49. Torres, V. I., Godoy, J. A. & Inestrosa, N. C. Modulating Wnt signaling at the root: Porcupine and

Wnt acylation. *Pharmacol. Ther.* **198**, 34–45 (2019).
50. Hofmann, K. A superfamily of membrane-bound O -acyltransferases with implications for Wnt signaling. *Trends Biochem. Sci.* **25**, 111–112 (2000).
51. Zhong, Z. *et al.* PORCN inhibition synergizes with PI3K/mTOR inhibition in Wnt-addicted cancers. *Oncogene* **38**, 6662–6677 (2019).
52. Madan, B. *et al.* Wnt addiction of genetically defined cancers reversed by PORCN inhibition. *Oncogene* **35**, 2197–2207 (2016).
53. García-Reyes, B. *et al.* Discovery of Inhibitor of Wnt Production 2 (IWP-2) and Related Compounds As Selective ATP-Competitive Inhibitors of Casein Kinase 1 (CK1) δ/ε. *J. Med. Chem.* **61**, 4087–4102 (2018).
54. Alfarouk, K. O. *et al.* Resistance to cancer chemotherapy: failure in drug response from ADME to P-gp. *Cancer Cell Int.* **15**, 71 (2015).
55. Garg, H., Suri, P., Gupta, J. C., Talwar, G. P. & Dubey, S. Survivin: a unique target for tumor therapy. *Cancer Cell Int.* **16**, 49 (2016).
56. Rodon, J. *et al.* Phase 1 study of single-agent WNT974, a first-in-class Porcupine inhibitor, in patients with advanced solid tumours. *Br. J. Cancer* **125**, 28–37 (2021).
57. Tabernero, J. *et al.* A Phase Ib/II Study of WNT974 + Encorafenib + Cetuximab in Patients With BRAF V600E -Mutant KRAS Wild-Type Metastatic Colorectal Cancer. *Oncologist* **28**, 230–238 (2023).
58. Moisan, F. *et al.* Enhancement of paclitaxel and carboplatin therapies by CCL2 blockade in ovarian cancers. *Mol. Oncol.* **8**, 1231–1239 (2014).
59. MABUCHI MIYUKI. Systematic Trial for Evaluating Docetaxel in a Human Prostate Cancer Cell DU145 Xenograft Model. *Anticancer Res.* **37**, 1665–1676 (2017).
60. Yun, E.-J. *et al.* Targeting Cancer Stem Cells in Castration-Resistant Prostate Cancer. *Clin. Cancer Res.* **22**, 670–679 (2016).
61. Abreu de Oliveira, W. A. *et al.* Wnt/β-Catenin Inhibition Disrupts Carboplatin Resistance in Isogenic Models of Triple-Negative Breast Cancer. *Front. Oncol.* **11**, (2021).
62. Matikas, A. *et al.* Dynamic evaluation of the immune infiltrate and immune function genes as predictive markers for neoadjuvant chemotherapy in hormone receptor positive, HER2 negative breast cancer. *Oncoimmunology* **7**, e1466017 (2018).
63. Kimbung, S. *et al.* Assessment of early response biomarkers in relation to long-term survival in patients with HER2-negative breast cancer receiving neoadjuvant chemotherapy plus bevacizumab: Results from the Phase II PROMIX trial. *Int. J. Cancer* **142**, 618–628 (2018).
64. Tempfer, C. Basal-like molecular subtype and HER4 up-regulation and response to neoadjuvant chemotherapy in breast cancer. *Oncol. Rep.* (2011) doi:10.3892/or.2011.1392.
65. Driehuis, E., Kretzschmar, K. & Clevers, H. Establishment of patient-derived cancer organoids for drug-screening applications. *Nat. Protoc.* **15**, 3380–3409 (2020).
66. Wensink, G. E. *et al.* Patient-derived organoids as a predictive biomarker for treatment response in cancer patients. *npj Precis. Oncol.* **5**, 30 (2021).
67. Sachs, N. *et al.* A Living Biobank of Breast Cancer Organoids Captures Disease Heterogeneity. *Cell* **172**, 373-386.e10 (2018).
68. Shang, S. *et al.* Chemotherapy-Induced Distal Enhancers Drive Transcriptional Programs to Maintain the Chemoresistant State in Ovarian Cancer. *Cancer Res.* **79**, 4599–4611 (2019).
69. Wang, L. *et al.* Chromatin accessibility regulates chemotherapy-induced dormancy and reactivation. *Mol. Ther. - Nucleic Acids* **26**, 269–279 (2021).
70. Chera, S. *et al.* Apoptotic Cells Provide an Unexpected Source of Wnt3 Signaling to Drive Hydra Head Regeneration. *Dev. Cell* **17**, 279–289 (2009).
71. Wang, W. *et al.* ABL1-dependent OTULIN phosphorylation promotes genotoxic Wnt/β-catenin

activation to enhance drug resistance in breast cancers. *Nat. Commun.* **11**, 3965 (2020).
72. Ince, T. A. *et al.* Characterization of twenty-five ovarian tumour cell lines that phenocopy primary tumours. *Nat. Commun.* **6**, 7419 (2015).
73. Bolger, A. M., Lohse, M. & Usadel, B. Trimmomatic: a flexible trimmer for Illumina sequence data. *Bioinformatics* **30**, 2114–2120 (2014).
74. Dobin, A. *et al.* STAR: ultrafast universal RNA-seq aligner. *Bioinformatics* **29**, 15–21 (2013).
75. Liao, Y., Smyth, G. K. & Shi, W. featureCounts: an efficient general purpose program for assigning sequence reads to genomic features. *Bioinformatics* **30**, 923–930 (2014).
76. Love, M. I., Huber, W. & Anders, S. Moderated estimation of fold change and dispersion for RNA-seq data with DESeq2. *Genome Biol.* **15**, 550 (2014).
77. Desmedt, C. *et al.* Biological Processes Associated with Breast Cancer Clinical Outcome Depend on the Molecular Subtypes. *Clin. Cancer Res.* **14**, 5158–5165 (2008).
78. R Core Team. R: A language and environment for statistical computing. (2021).

AUTHOR CONTRIBUTIONS

YEL, WO, and FL conceived and designed the study. WO partially carried out flow cytometry experiments, RT-qPCR experiments, analysis of publicly available datasets. AP performed all bioinformatic and biostatistical analyses under the supervision of FR and CD. AQ partially carried out flow cytometry experiments, western blot analysis, RT-qPCR experiments, and *in vivo* experiments. FR provided critical input for the bulk transcriptomic analysis under supervision of and in consultation with CD. PA participated in library preparations for mRNA-seq samples and provided input in experimental design. CL and WDW provided aid in the *in vivo* experiments under supervision of SS and DA. LM provided aid for the culturing and maintenance of patient derived organoid (PDO) models. SH provided input and feedback into experimental design under supervision of AB. SM generated the *in vitro* cell line, PDC-BRC-101. AdJS provided critical input in experimental design and assisted in the generation of several fluorescent reporter cell lines. MB provided input in the *in vivo* experimental design. SJS provided critical input in human patient dataset analysis. CS provided the PDO models. AB provided critical input for experimental design. DA provided critical input in *in vivo* data analysis. YEL carried out the remainder of the experimental work. Data analysis and figure preparation were performed by YEL and WO and reviewed by FL. The manuscript was written by YEL and FL and reviewed and approved by all authors. FL secured funding and supervised and guided experimental work and manuscript preparation.

ACKNOWLEDGEMENTS

We are grateful to the KU Leuven FACS core team for providing the facility. We also thank the KU Leuven Genomics Core (http://genomicscore.be) for RNA sequencing, and data processing. We also thank the KU Leuven TRACE core and the MOSAIC core for help in *in vivo* experimental design and animal imaging. The authors would like to extend their gratitude to the FWO Research Foundation – Flanders for the Ph.D. fellowships awarded to P.A. (11M7822N). AdJS was supported by PhD Emmanuel van der Schueren (EvdS) fellowship granted by Kom Op Tegen Kanker (KOTK) and a Postdoctoral Mandate (PDM) granted by KU Leuven. The Lluis Lab is financed by the FWO Research Project Grants G091521N (AB, DA, FLL), G073622N (FLL), and the C1 KU Leuven internal grant C14/21/115 (FLL).

MATERIALS AND METHODS

Ethics declaration

All xenograft animal experiments performed were approved by the Ethics Committee at KU Leuven University under the ethical approval codes P055/2022 and P016/2023.

Patient derived organoid (PDO) models used in this study were established from freshly resected tumor tissues obtained from TNBC patients at the Antoni van Leeuwenhoek Hospital. The study was approved by the institutional review board (NKI-B17PRE) and the subjects provided informed consent.

All cell lines used in this study are approved for use by the Ethics Committee at the KU Leuven University Biobank under the code S65166.

TNBC cell line culture

MDA-MB-231 (ATCC-HTB-26) and MDA-MB-468 (ATCC-HTB-132) were maintained in DMEM high glucose (Gibco, 41965039) supplemented with 10% (v/v) fetal bovine serum, 1mM sodium pyruvate (Gibco, 11140035), 100µg/mL penicillin-streptomycin (Gibco, 15140163), and 0.01mM 2-mercapthoethanol (Gibco, 31350010).

PDC-BRC-101 cell line (PDX-derived cell line) was obtained from collaborators, Daniela Anibali and Stijn Moens (Amant Lab – Gynecological Oncology) – KU Leuven and maintained in OCMI media[72] composed of a composed of 1:1 mixture of Medium199 (Gibco, 31150022) and DMEM F-12 (Gibco, 11320074) supplemented with 10% (v/v) fetal bovine serum, 100µg/mL penicillin-streptomycin, 20µg/mL insulin (Sigma/Merck, I9278), 25ng/mL cholera toxin subunit B (Sigma/Merck, C9903-.5MG), 0.5µg/mL hydrocortisone (Sigma/Merck, H0888-1G), and 10ng/mL epidermal growth factor (Stem Cell Technologies, 78006.1).

All cell lines were cultured in 84mm x 20mm (D x H) tissue-culture treated dishes at 37°C and 5% CO_2 and maintained at 70-80% confluency. For cell line passaging and plating, 1X phosphate-buffered saline (Gibco, 10010-015) was used as a washing solution followed by dissociation using 0.25% trypsin-EDTA (Gibco, 25200-056) and cell-pelleting by centrifugation for 4 minutes at 300G (0.3rcf). Cells were counted manually via the BRAND counting chamber Neubauer improved (Sigma Aldrich/Merck, BR717810-1EA) under a 10X objective lens using a Leica DMi inverted microscope. The same microscope, equipped with a 2.5 Megapixel HD Microscope Camera Leica MC120 HC, was used to obtain images of cultured cancer cell lines. Unless specified otherwise, cancer cell lines were plated according to the following seeding densities: $7.3\,x\,10^3\ \frac{cells}{cm^2}$ and $10.5\,x\,10^3\ \frac{cells}{cm^2}$ (MDA-MB-231 and MDA-MB-468/PDC-BRC-101, respectively).

Chemotherapeutic treatment of TNBC cell lines and PDO models

Cell lines were treated with increasing concentrations of docetaxel (Taxotere, 0–144 nM) and carboplatin (Carbosin, 0–1600 µM) for 72h. Cell metabolic activity, reflecting cell-number and -viability) was assessed using the MTT [Thiazolyl Blue Tetrazolium Bromide] assay (Sigma/Merck, M5655-500mg) according to manufacturer's instructions and sigmoidal dose-response curves were generated to calculate the mean

IC50 values of each drug that were used in the subsequent study. Chemotherapeutic agents were obtained from the pharmacy of Universitair Ziekenhuis (UZ) Leuven.

Lentiviral particle production and transduction

Lentiviruses were produced according to the RNAi Consortium (TRC) protocol available from the Broad Institute (https:// portals.broadinstitute.org/gpp/public/resources/protocols). In brief, $7\,x\,10^5$ HEK-293T cells were seeded per well in 6-well plates and transfected the following day with 750 µg pCMV-dR8.91, 250 µg pCMV-VSV-G, and 1 µg of the specific lentiviral plasmid/construct using FugeneHD (Promega, E2311) in Optimem (Gibco, 31985070). One day after, the culture medium was refreshed. The same day, lentivirus-recipient cells were plated in 6-well plates at their respective concentrations (see cell line culture). Lentivirus-containing medium was collected from HEK293T cells 48h and 72h post-transfection and added to recipient cancer cells after filtration using a 0.45 µM filter (VWR-Corning, 431220). 48h post infection, recipient cancer cells were washed thoroughly with PBS, medium refreshed, and the appropriate selection antibiotics applied until selection process was completed.

Wnt-transcriptional reporters, TOPGFP (7xTOP-GFP), TOPFLASH (7xTcf-FFluc), and mCherry-TOPGFP (7xTOP-GFP.mC) were obtained from Addgene (#35489, #24308, and #35491, respectively). Wnt-transcriptional reporter dTOPGFP was gifted to us from the Moon lab University of (Washington – USA).

For PORCN shRNA mediated silencing, we used the MISSION® Lentiviral shRNA (Sigma Aldrich/Merck, SHCLNG – clones, TCRN000153848 and TCRN000157366) and the MISSION pLKO.1-puro Non-Target shRNA Control Plasmid DNA (SHC016-1EA) as a negative control in experiments.

Real-Time Quantitative Polymerase Chain Reaction and Gene Expression Analysis

For RT-qPCR, total RNA was extracted (from TNBC cell lines or cryopreserved tumor tissue) using the GenElute mammalian total RNA miniprep kit (Sigma/Merck, RTN350-1KT) according to manufacturer's instructions with an additional step of DNA digestion using the On-Column DNAse I digestion set according to manufacturer's instructions (Sigma/Merck, DNASE70). cDNA was synthesized from 500 ng of total RNA using the BIORAD iScript cDNA cDNA synthesis kit (BIORAD, CAT#1708891), according to manufacturer's instructions. Quantitative real-time PCR reactions were set up in technical triplicates with Platinum SYBR Green qPCR SuperMix-UDG (Invitrogen, 11733-046) on a ViiA7 Real-Time PCR System (Thermo-Scientific). Expression levels were normalized to two housekeeping genes (HK) RPL19 and GAPDH to determine ΔCT values. Statistical testing of differences in expression levels between samples was carried out based on relative-expression values ($2^{-\Delta CT}$). In some figures, gene expression values are represented as fold-change for convenience of interpretation, although statistical testing was performed on relative expression values ($2^{-\Delta CT}$).

SDS-PAGE and Western Blot analysis

TNBC cell lines were washed with PBS and collected/pelleted by centrifugation. Whole cell lysates were obtained via mechanical lysis using a needle (VWR-TERUMO, AN2138R1) and RIPA cell lysis buffer (Sigma/Merck, R0278-50mL) supplemented with a cocktail of 1:100 phosphatase inhibitors cocktail 2 and 3 (Sigma/Merck, P5726-1ML and P0044-1ML, respectively) and 1:100 protease inhibitor cocktail (Sigma/Merck, 11873580001). Samples were placed on a rotation wheel for a minimum of 30 minutes at

4 °C after which they were centrifuged at 16,000x g for 10 minutes at 4 °C. The supernatant from the lysates was collected and protein concentration was determined using the Bradford Assay (Biorad, 5000006). For SDS-PAGE 20 mg of protein were mixed with 4x Laemmli buffer (240 mM Tris/HCL pH 6.8, 8% SDS, 0.04% bromophenol blue, 5% 2-mercaptoethanol, 40% glycerol) and denatured for 5 minutes at 95°C prior to electrophoretic protein separation. Resolved protein extracts were transferred to PVDF membranes (BIORAD, 162-0177). Transfer success was assessed with Ponceau S solution, and membranes were blocked with 5% non-fat milk or 5% BSA in TBS-T (0.1% Tween-20®) for 60 minutes. After blocking, membranes were incubated with primary antibodies at 4°C overnight. The day after, membranes were washed 3 times with PBS-T for 10 minutes and incubated with secondary HRP-conjugated antibodies. Immunolabeled proteins were detected with Supersignal West Pico chemiluminescent kit (Fisher Scientific, 34077) on autoradiography film (Santa Cruz, SC-201697). The primary antibodies used were active rabbit anti-non-phosphorylated β-catenin (CellSignaling Technologies, #19807S), rabbit anti-PORCN (Novus Biologicals, NBP1-59677), and rabbit anti-WNT2b (Abcam, ab178418). Mouse anti-β-Actin (Santa Cruz Biotechnology; sc-47778) was used as a loading control.

Flow Cytometry

For Wnt-activation assessment, cells were washed with PBS and collected/pelleted by centrifugation. Cells were resuspended in PBS2%FBS, counterstained with 5µg of 4',6-diamidino-2- phenylindole (DAPI – 1:1) (Sigma/Merck, D9542-10mg) to eliminate dead cells before running through the flow cytometer. Cell lines lacking any of the previously described Wnt-transcriptional reporters were used as gating controls.

For ALDH activity assay, cells were washed with PBS and collected/pelleted by centrifugation. Cells were stained using the AldeRed ALDH detection assay (Sigma/Merck, SRC150) according to manufacturer instructions. Cells were counterstained with 5µg of DAPI (1:1) to eliminate dead cells before running through the flow cytometer.

For Annexin V apoptosis analysis, cells were washed with PBS and collected/pelleted by centrifugation. Cells were resuspended in 1x Annexin V binding buffer (BD Pharmigen, 51-66121E) and incubated at room temperature in the dark for 15 minutes with APC-conjugated Annexin V (Thermo-eBioscience, BMS306APC-100). After incubation, cells were diluted in 1X binding buffer supplemented with 100 nM of DAPI before running through the flow cytometer. Unstained and single-stained (Annexin V-only or DAPI-only stained) cells were used as gating controls.

To obtain chemotherapy-induced Wnt^{High} and Wnt^{Low} cells, cells were washed with PBS and collected/pelleted by centrifugation. Cells were resuspended in PBS4%FBS, counterstained with 5µg of DAPI (1:1) to eliminate dead cells before running through the SONY MA900 Multi-Application Cell Sorter. Depending on the application, $2 - 3\ x\ 10^5$cells were sorted (based on their GFP expression) into 1.5mL Eppendorf tubs (with 300µl of PBS4%FBS) and either used for RNA-extraction and gene expression analysis or for re-culturing.

For immunostaining of active- (non-phosphorylated) β-catenin, cells were washed with PBS and collected/pelleted by centrifugation. Cells were fixed with ice-cold 70% Ethanol. After which samples were with PBS2%FBS and blocked with 5% donkey serum (in PBS) at room temperature for 30-60 minutes. Cells were re-pelleted by centrifugation, washed with PBS2%FBS and incubated with active rabbit anti-non-

phosphorylated β-catenin antibody at room temperature for 60 minutes. Cells were re-pelleted by centrifugation, washed with PBS2%FBS and incubated with a conjugated secondary (donkey anti-rabbit – Alexa-647 – Thermo-Life tech, A31573) in the dark at room temperature for 30 minutes. Cells were re-pelleted by centrifugation, washed with PBS2%FBS and counterstained with 5µg of DAPI (1:1) before running through the flow cytometer. Unstained and single-stained (secondary antibody-only stained) cells were used as gaiting controls.

Unless specified otherwise, all data were collected on a BD FACS Canto II at the KU Leuven Flow Cytometry Core and analyzed using FlowJo v.10.6.2.

Conditioned media and co-culture analysis

Conditioned media (CM) was collected from TNBC cell lines recovering from chemotherapy treatment (5 days of treatment and 1 week of recovery) and filtered using a 0.45µM filter to ensure removing cell-debris. Filtered CM as concentrated 20x (20mL to 1mL) using Vivaspin centrifugal concentrator column with a molecular weight cutoff of 50kDa (Sigma Aldrich, Z614645-12EA). Filtered media was centrifuged for 45 minutes at 4°C. Concentrated CM was added to chemo-naïve TNBC cell lines for 48h in a 1:1 dilution (Concentrated CM:basal culture cancer media) and Wnt-activation levels were evaluated using FACS.

For co-culture experiments, MDA-MB-231 cell line was treated with either chemotherapeutic agent for 72h after which treatment was stopped and an equal number of chemo-naïve MDA-MB-231-TGP.mC cells was plated in the same dish and cultured in basal culture cancer media. After 72h of co-culture, Wnt-activation levels in the MDA-MB-231-TGP.mC cell line was evaluated using FACS.

Cell line derived xenograft establishment and *in vivo* live imaging analysis

$1\ x\ 10^6$ MDA-MB-231 TOPFLASH cells were engrafted subcutaneously (1:1 PBS: growth-factor reduced Matrigel) into the right flank of female NMRI-Foxn1 mice (4-6 weeks old) to form a solid tumor. Upon observation of visible/palpable solid growth, tumor volumes were measured using digital calipers (and calculated as $L\ x\ W\ x\ \frac{\pi}{6}$; L: length and W: width). Animals were randomly assigned to one of three (or six) treatment groups (n = 7-8 mice per group) with an average tumor volume of 150mm^3 per group. Docetaxel (15mg/kg) and Carboplatin (100mg/kg) were administered via intraperitoneal (IP) injection once weekly (1 cycle) for a total of three cycles. LGK-974 (2mg/kg) was administered daily via oral gavage for a total of 3 cycles (3 weeks). For assessment of Wnt-activation dynamics, animals were subjected to live-bioluminescent imaging before-, 24 h-, 48h-, and 72h- after chemotherapeutic administration. For live-bioluminescent imaging, animals were injected (IP) with the luciferase substrate D-luciferin (200µL of 15mg/ml - assuming an average animal weight of 24-26gr) (Perkin Elmer, 122799) and incubated for 10 minutes at room temperature before images were taken using IVIS Spectrum In Vivo Imaging System (Perkin Elmer). Wnt-activation signal was calculated as the bioluminescent signal captured by the IVIS Spectrum normalized to the tumor volume recorded per animal. Analysis of bioluminescent images was performed via the Aura software v.4.0.0. Tumor volume was recorded every 48h and body weight was closely monitored throughout the treatment course and recorded every 72-96h using an automatic scale. All animals were euthanized at the end of the treatment course and tumors (when available) were resected/collected for downstream analyses.

RECIST Analysis

RECIST analysis was performed using tumor volumes measured and recorded (as described previously) at the onset of treatment and at the end of treatment (day of sacrifice). Relative tumor volume (RTV) was calculated by dividing the recorded volume at the end of treatment by the recorded volume at the onset of treatment. Response to therapy was based on the RECIST-based criterion: Complete response (CR), Partial response (PR), Stable disease (SD), and Progressive disease (PD); CR: RTV = 0, PR: $0 < RTV \leq 0.657$, SD: $0.657 < RTV \leq 1.728$, PD: $RTV > 1.728$.

Tumorsphere Formation Assay

Cells were washed with PBS and collected/pelleted by centrifugation. Cells were resuspended in PBS4%FBS, counterstained with 5µg of DAPI (1:1) to eliminate dead cells before running through the SONY MA900 Multi-Application Cell Sorter. $1\ x\ 10^3$single cells were sorted (based on their GFP expression) directly in ultra-low attachment 6-well plates (Fisher-Corning, 10154431) cultured in serum-free tumorsphere assay medium composed of DMEM/F12 (Gibco, 11320074), 1X B27 (Thermo-Scientific, 12587010), 10ng/mL basic fibroblast growth factor (bFGF) (Peprotech, 100-18b), 20ng/mL EGF (Peprotech, AF-100-15), and 2% growth-factor reduced Matrigel (Corning, 734-0268). Sorted cells were allowed fourteen days to grow, at the end of which, spheres were collected and centrifuged at 50g for 10minutes, resuspended gently, and transferred to 96-well plates (Fisher-Falcon,353072). Plates were briefly centrifuged at 50g for an additional 1 minutes to pull down larger spheroid (>60 µm) which were counted under a microscope (10X) using a tally counter.

Next-Generation mRNA Sequencing

Total RNA was obtained from cells using the GenElute mammalian total RNA miniprep kit (Sigma, RTN350-1KT). RNA-sequencing (RNA-seq) libraries were prepared using 750 ng of total RNA using the KAPA stranded mRNAseq kit (Roche, 8098123702) according to the manufacturer's specifications. 100 nM of KAPA-single index adapters (Roche, KK8702) were added to the A-tailed cDNA and the libraries underwent 10 cycles of amplification. Agentcourt AMPure XP beads (Beckman Coulter, A63880) were used for the 1X library clean-up. The fragment size of the libraries was assessed using the Agilent Bioanalyzer 2100 with the High Sensitivity DNA kit (Agilent, 5067-4626). The concentration of the libraries was measured by the High Sensitivity QuBit kit (Invitrogen, Q33230). Each library was diluted to 4 nM and pooled for single-end 50-bp sequencing on an Illumina Hiseq4000 with 20 – 27 million reads per sample (22 million reads on average).

Bulk mRNA-sequencing analysis

FASTQ files generated from the sequencing (Sequencing run Fig. 1 and Fig. 3) were sent for downstream processing. Adapters were trimmed using Trimmomatic[73] v0.39 and the trimmed FASTQ file was aligned to the GRCh38 genome (hg38) using the STAR aligner[74] v2.7.10. Gene counts, gene annotation and sample read characteristics were obtained by applying standard filters within featureCounts[75] from the subread package v2.0.3. Gene counts were then normalized using the variance stabilizing transformation (VST). Z-scores used to describe the gene expression distribution across samples were calculated using median absolute deviation whole the heatmaps comparing z-scores between samples were created using pheatmap v1.0.12. Differential gene expression analysis was performed using DESeq2[76] and batch effects were accounted for in the (Wnt^{High} vs. Wnt^{Low} cohort). Volcano plots were created using EnhancedVolcano v1.18.0 using custom settings of FCcutoff = 0.6 and pCutoff = 0.05. Gene set variation analysis was

performed using GSVA v1.48.3. Signature scores for the Caspase 3/Apoptosis[77] and diapause/DTP signatures (Supplementary Table 4) were calculated after the gene counts were transformed using both log2(x) +1 and VST methods. Box plots comparing the signature score(s) distribution between Wnt^{High} and Wnt^{Low} samples between treatment conditions were created using ggplot2 v3.4.3. Forest plots for regression analysis were created using forestplot v3.1.3. Analyses following the gene count extraction were all performed in R[78] v4.3.0.

Functional Enrichment Analysis of publicly available datasets

Datasets GSE87455 and GSE21974 were downloaded from the GeneExpression Omnibus and ArrayExpress public repositories, respectively. Differentially expressed genes with |log2(fold-change)| >1 and p-value < 0.05 were obtained using limma (v3.26.8) R package in R (v4.02) and by using the limma method on NetworkAnalyst (39). Differentially expressed genes were ranked by fold-change for Gene Set Enrichment Analysis (GSEA v4.1.0) using the weighted enrichment statistic for Hallmark and KEGG gene sets from the human MSigDB database. The statistical significance threshold was set at FDR<0.1 or ($p<0.5 \wedge FDR<0.25$)

Patient derived organoid culture, treatment, and analysis

R1-IDC113 and R2-IDC159A PDO lines were gifted by our collaborator, Laboratory of Colinda Scheele – VIB-KU Leuven. Both PDO lines were maintained in growth factor reduced type 2 Cultrex (Biotechne/R&D Systems, 3533-010-02) with phenol red-free DMEM/F-12, HEPES (Gibco, 11039021) supplemented with 10mM Nicotinamide (Sigma/Merck, N0636-100G), 1.25mM N-acetyl-L-cystine (Sigma/Merck, A9165-5G), 500ng/mL Hydrocortisone, 100nM β-estradiol (E8875-250MG), 500nM SB202190 (Stem Cell Technologies, 72632), 500nM A83-01 (Stem Cell Technologies, 72022), 5uM Y-27632 (Stem Cell Technologies, 72304), 50µg/mL Primocin (Invivogen, ant-pm-05), 10µM Forskolin (Sigma/Merck, F3917-10MG), 1X B27 (50X – ThermoFisher Scientific, 17504044), 100ng/mL r-Noggin (Stem Cell Technologies, 78060), 5ng/mL FGF-10 (Stem Cell Technologies, 78037), 37.5 ng/mL Heregulin B-1 (Peprotech, 100-03), 5ng/mL EGF, 5ng/mL FGF-7 (Peprotech, 100-19), and 100µg/mL penicillin-streptomycin.

Both PDO lines were cultured in 24 well cell culture microplates – 22 mm x 20 (D x H) – at 37°C and 5% CO_2 and maintained at 70-80% confluency. For passaging and plating, (ice-cold) 1X phosphate-buffered saline (Gibco, 10010-015) was used to wash and dissociate the BME followed by single cell enzymatic dissociation using 0.05% trypsin-EDTA (Gibco, 25200-056) and cell-pelleting by centrifugation for 5 minutes at 1500 rpm (4°C). Cells were counted manually via the BRAND counting chamber Neubauer improved (Sigma Aldrich/Merck, BR717810-1EA) under a 10X objective lens using a Leica DMi inverted microscope. The same microscope, equipped with a 2,5 Megapixel HD Microscope Camera Leica MC120 HC, was used to obtain images of cultured PDO-lines. Unless specified otherwise, both PDO models were plated according to the following seeding density: $5.9\ x\ 10^2\ \frac{cells}{mm^2}$

To determine working chemotherapy drug concentrations, PDO lines were treated with increasing concentrations of docetaxel (Taxotere, 0.0625–512 nM) and carboplatin (Carbosin, 0 – 1600 µM) for 96h. Cell metabolic activity, reflecting cell-number and –viability was assessed using the CellTiter-Glo® 3D Cell Viability Assay (Promega, G9682) and sigmoidal dose-response curves were generated to calculate the mean IC50 values of each drug that were used in the subsequent study. Chemotherapeutic agents were obtained from the pharmacy of Universitair Ziekenhuis (UZ) Leuven.

Statistical Analysis

All data were analyzed using GraphPad Prism (v8.0.1), except for mRNA-sequencing derived data and transcriptomic datasets. Unless otherwise specified, comparisons between two groups were tested for statistical significance using Unpaired t-tests. Comparisons between multiple groups were performed using a One-way analysis of variance (ANOVA). Comparisons between multiple groups across multiple time points were performed using Two-way ANOVA. All statistical testing was corrected for multiple comparisons, using the Holm-Sidak method when comparing samples based on experimental design. For the reader's convenience, all statistical tests and sample sizes are indicated in the figure legends.

For mRNA-sequencing derived data, regression analysis was performed to observe associations between outcomes (in-house gene signature scores/GSVA signature scores) and independent co-variate (Wnt^{High} vs. Wnt^{Low}) per treatment condition (CAR or DOC or UNT) using lqmm v.1.5.8 and quantreg v5.97 while accounting for batch effects.

Schematic Illustrations and artwork

All schematic illustrations were created using Biorender.com

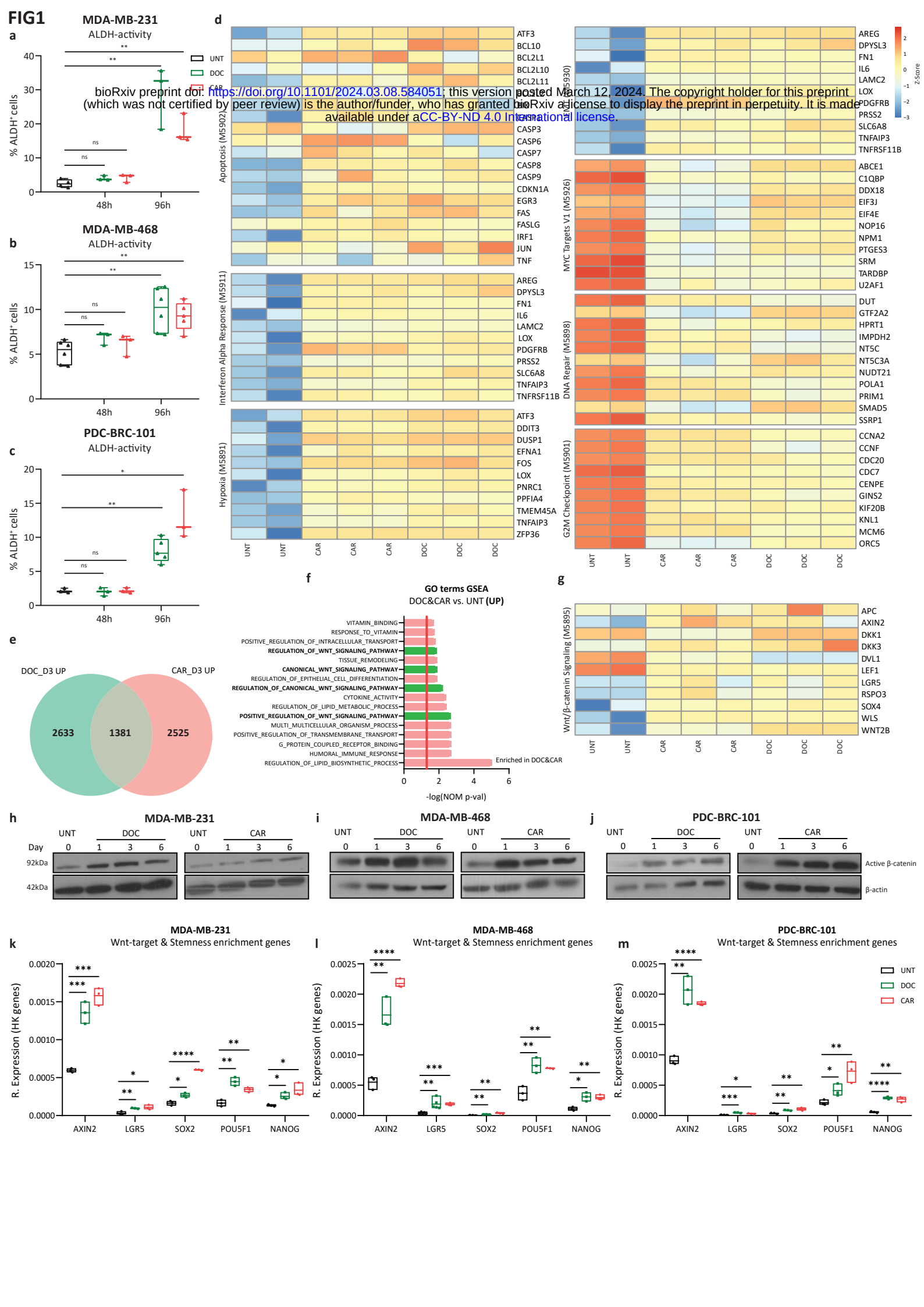

Figure 1: Wnt-transcriptional activation precedes drug-tolerant cell(s) enrichment upon chemotherapeutic treatment

a-c) Flow cytometry analysis displaying %ALDH⁺ cells of MDA-MB-231 (top), MDA-MB-468 (middle), and PDC-BRC-101 (bottom) cell lines treated with DOC (4.5nM) or CAR (35uM, 25uM, 35uM for each cell line, respectively) for 48h and 96h. Multiple t-tests corrected for multiple comparisons using the Holms-Sidak method (n = 3 independent experiments). All data points shown from min. to max. (box and whiskers). **d)** Normalized gene expression heatmaps displaying (≈12-20) selected genes (based on DEGs predicting each representative process and/or hallmark) representing different processes and signaling cascades deregulated (relative to UNT cells) in MDA-MB-231 cell line treated with DOC or CAR for 72h. The pro[illegible]analyzed by one-tailed GSEA ranked by Normalized Enrichment Score (NES) – Supplementary Fig. S1j, k. **e)** Venn diagram indicating commonly upregulated (1381) genes between DOC (2633) and CAR (2525) treatment (vs. UNT). **f)** Enriched processes from Gene Ontology (GO) terms databases analyzed by one-tailed GSEA ranked by a positive NES and based on commonly upregulated genes between DOC and CAR treatment. Red line indicates significance threshold value, (-log(NOM p-val) = 1.3) and highlighted bars indicate GO terms linked to Wnt/β-catenin signaling regulation. **g)** Normalized gene counts heatmap displaying (11) selected genes representing Wnt/β-catenin signaling in MDA-MB-231 cell line treated with DOC and CAR for 72h. Genes selected for heatmap **g** were based on Wnt/β-catenin signaling Hallmark – GSEA. Data used to generate panels **d-g** was obtained from mRNA-sequencing of MDA-MB-231 cell line treated with DOC or CAR for 72h). **h-j)** Western blot analysis of active- (non-phosphorylated) β-catenin in MDA-MB-231, MDA-MB-468, and PDC-BRC-101 cell lines treated with DOC or CAR for 1, 3, or 6 days. **k-m)** Gene expression levels obtained via RT-qPCR of Wnt-targets (AXIN2 and LGR5) and stem cell markers (SOX2, POU5F1, and NANOG) in MDA-MB-231, MDA-M-468, and PDC-BRC-101 cell lines treated with DOC or CAR for 72h, displayed as relative expression values (relative to housekeeping genes – HK-genes). Multiple t-tests corrected for multiple comparisons using the Holms-Sidak method (n = 3 independent experiments). All data points shown from min. to max. (box and whiskers). p values are indicated as *p < 0.05, **p < 0.01, ***p < 0.001, ***p < 0.0001, and ns, not significant.

FIG2

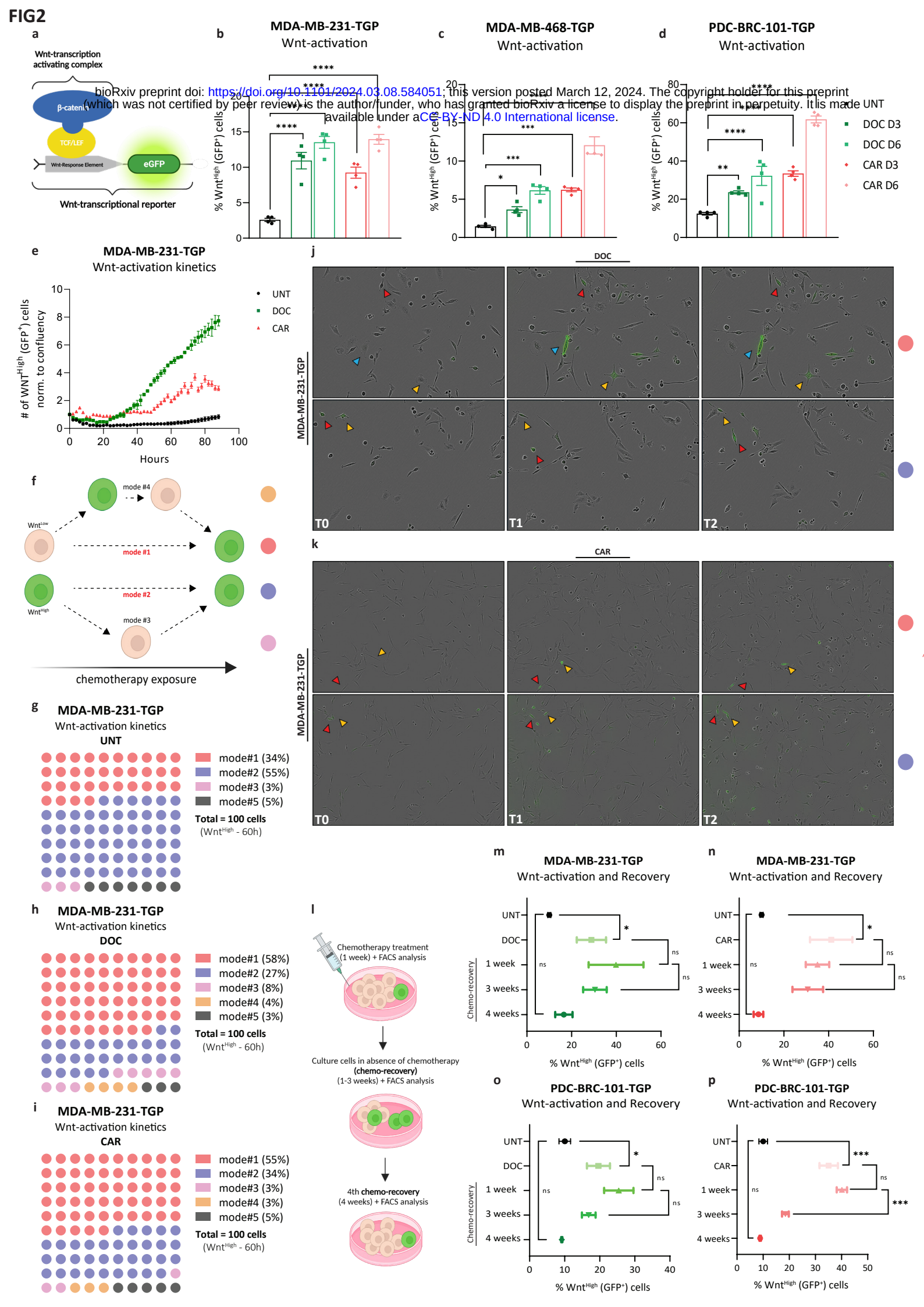

Figure 2: Induction of transient *de novo* Wnt signaling transcriptional activation in response to chemotherapy in TNBC cell lines

a) Schematic representation of Wnt/β-catenin-transcriptional reporter (TOPGFP). **b-d)** Flow Cytometry analysis displaying % of Wnt^{High} (GFP^{+}) cells for MDA-MB-231-TGP, MDA-MB-468-TGP, and PDC-BRC-101-TGP cell lines treated with DOC or CAR for 3 and 6 days. One-way ANOVA corrected for multiple comparisons using the Holms-Sidak method (n = 4 independent experiments). Data are presented as Mean ± SEM. **e)** Number of Wnt^{High} (GFP^{+}) cells detected by live-cell imaging normalized to the confluency of the well (total number of cells recorded) for MDA-MB-231-TGP cell line treated with DOC or CAR. **f)** Schematic representation of different fluctuation dynamics of Wnt-activation – mode numbered and color coded. **g-h)** Live-imaging quantification of different possible mechanisms of chemotherapy-induced Wnt-activation in MDA-MB-231-TGP TNBC cell line UNT or treated with DOC or CAR. n = 100 cells tracked every 2h for 60h per treatment condition. Every single cell tracked is represented as a circle and color coded with the scheme shown in **f**. **j-k)** Snapshots of still-frames from time-lapse live imaging experiments of MDA-MB-231-TGP TNBC cell line treated with DOC (top) or CAR (bottom) presenting mode #1 and mode #2 (color coding in scheme shown in f. T_0 indicates 0h, T_1 indicates 30h, and T_2 indicates approx. 50h. Yellow, red, and blue arrows indicate the same cell followed over the treatment period spanning different images (horizontal). **l)** Schematic representation of the experimental setup for chemotherapy treatment and recovery. **m-p)** Flow Cytometry analysis displaying % of Wnt^{High} (GFP^{+}) cells for MDA-MB-231-TGP and PDC-BRC-101-TGP cell lines treated with DOC or CAR for 1 week followed by removal of chemotherapy for 1-, 3-, and 4-weeks post-recovery. Two-tailed unpaired t-test (n=3 independent experiments). Data are presented as Mean ± SEM. p values are indicated as *p < 0.05, **p < 0.01, ***p < 0.001, ****p < 0.0001, and ns, not significant.

FIG3

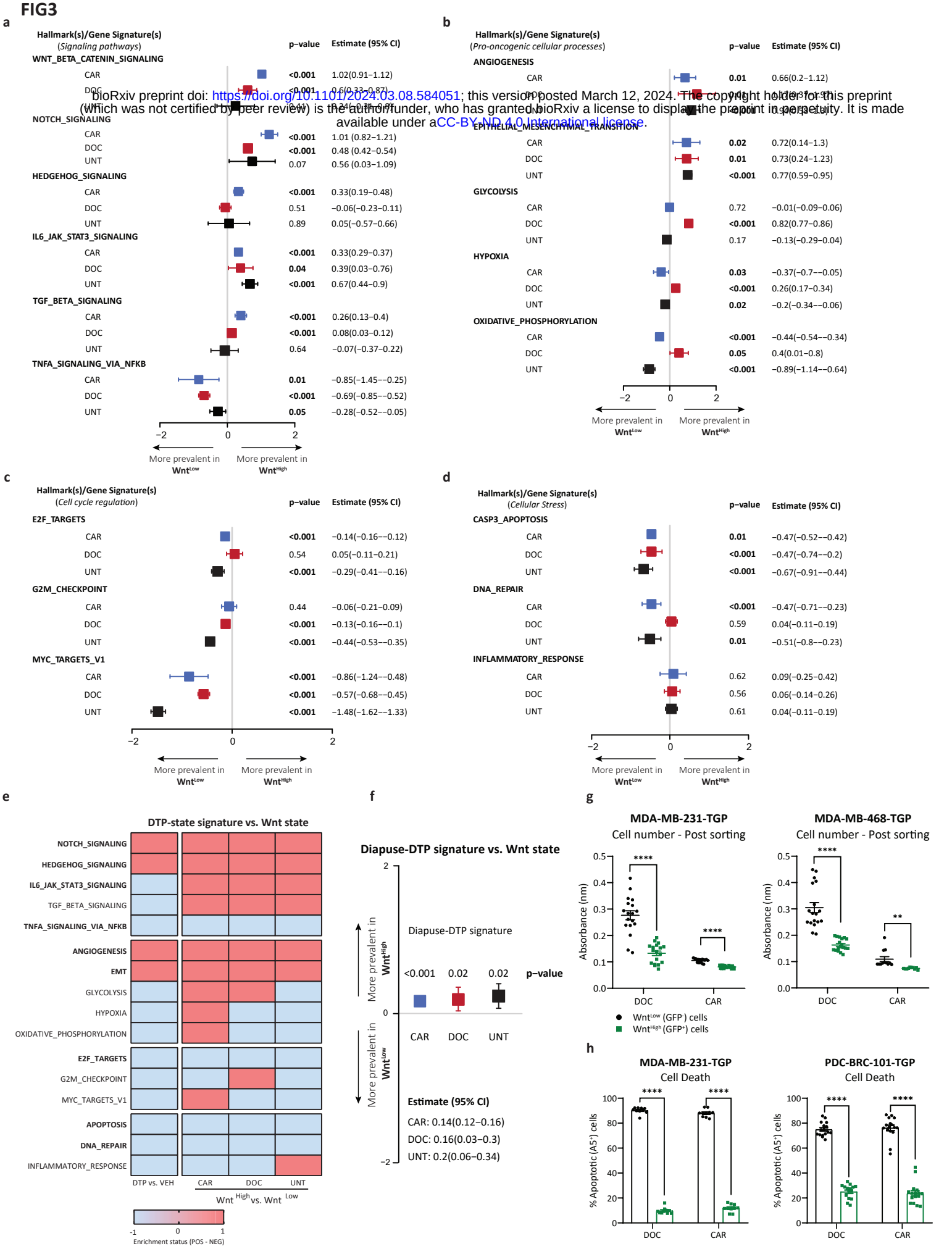

Figure 3: Bulk mRNA-sequencing of transcriptionally differential Wnt-populations reveals that chemotherapy-treated Wnt^{High} cells display DTP cell-properties

a-d) Forest plots depicting the association between gene signatures and Wnt-status of sorted Wnt^{High} vs. Wnt^{Low} obtained from samples treated with CAR or DOC or UNT samples. Gene signatures consist of in-house gene signatures[77] and Hallmark gene sets from MSigDB analysed using Gene set variation analysis (GSVA). Quantile regression was used to observe the median change in rescaled gene signatures after accounting for batch effects. Signatures having a non-zero positive estimate indicate increased activity in Wnt^{High} cells. **e)** Correlation analysis between transcriptional DTP cells[9] and Wnt-status of sorted Wnt^{High} vs. Wnt^{Low} cells obtained from samples treated with CAR or DOC and UNT samples. Enrichment status score of -1 (higher blue) indicates that a given hallmark/process is downregulated in DTPs or sorted Wnt^{High} cells while a score of 1 (red) indicates that a given hallmark/process is upregulated in DTPs or sorted Wnt^{High} cells. **f)** Forest plot depicting the association between Dia-pause-DTP signature[9] and Wnt-status of sorted Wnt^{High} vs. Wnt^{Low} cells obtained from samples treated with CAR or DOC and UNT samples. Analysis performed as in **a-d**. **g)** Absorbance values displaying cellular metabolic activity indicating cell number in sorted MDA-MB-231-TGP and MDA-MB-468-TGP cell lines 1 week after sorting (initial treatment before sorting was with DOC or CAR – 72h). Multiple t-tests corrected for multiple comparisons using the Holms-Sidak method (n = 3 independent experiments). Data are presented as Mean ± SEM. **h)** Flow cytometry analysis displaying % of Apoptotic (Annexin V^{+}) and their respective Wnt-status (% of Wnt^{High} (GFP^{+}) cells) of MDA-MB-231-TGP and PDC-BRC-101-TGP cell lines treated with DOC or CAR for 96h. Multiple t-tests corrected for multiple comparisons using the Holms-Sidak method (n = 5 independent experiments). Data are presented as Mean ± SEM. p values are indicated as *p < 0.05, **p < 0.01, ***p < 0.001, ****p < 0.0001, and ns, not significant.

FIG4

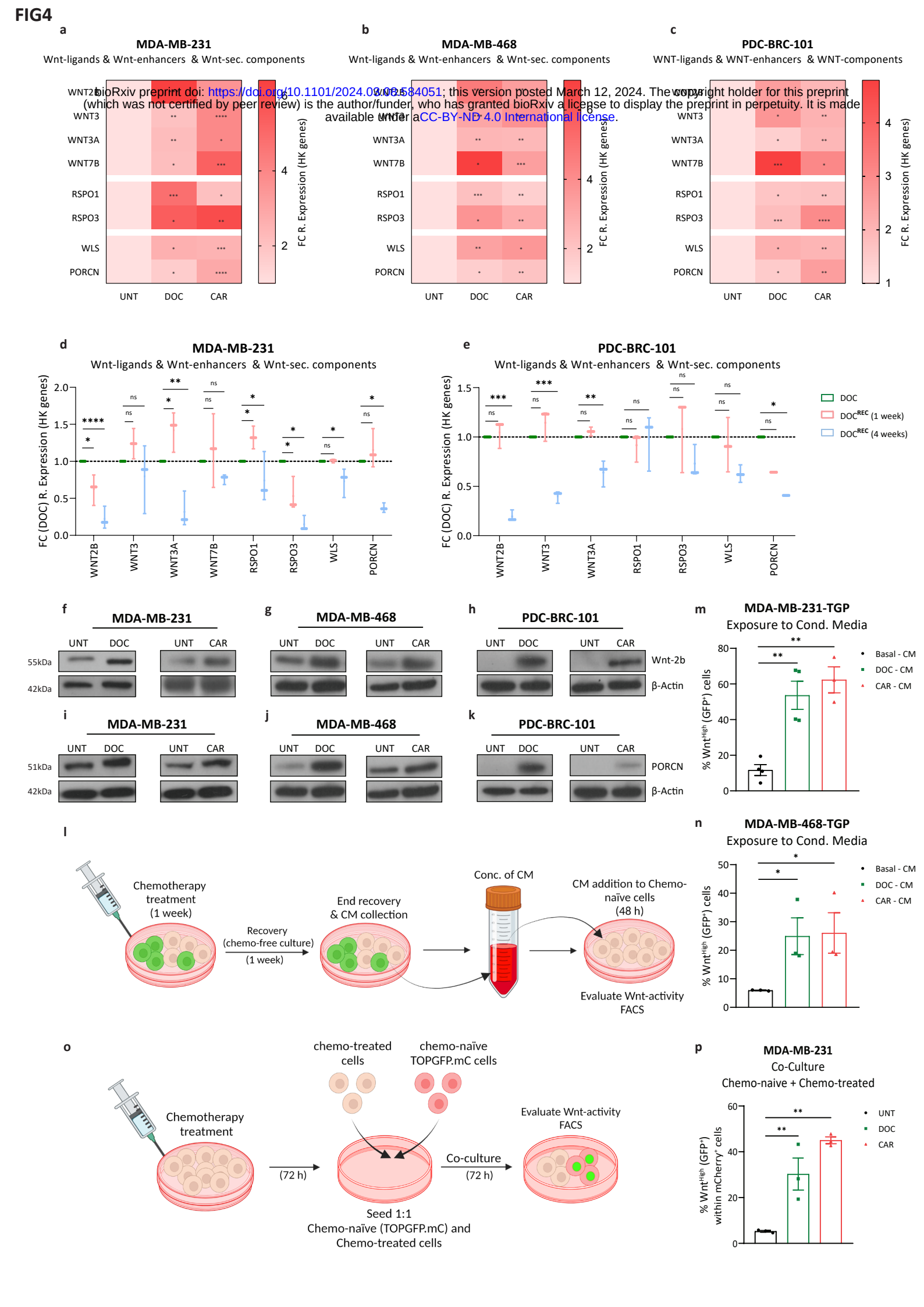

Figure 4: Chemotherapeutic treatment induces elevated transcriptional expression of Wnt ligands, Wnt enhancers, and Wnt secretion machinery components

a-c) Heatmaps showing gene expression levels obtained via RT-qPCR of Wnt ligands (WNT2B, WNT3, WNT3A and WNT7B), Wnt enhancers (RSPO1 and RSPO3), and Wnt ligand secretion machinery components (WLS and PORCN) for MDA-MB-231, MDA-MB-468, and PDC-BRC-101 cell lines treated with DOC or CAR for 72h, displayed as fold change (to UNT) of 2^{-dCt} values (relative to HK-genes). Unpaired t-tests based on relative expression values (2^{-dCt}) (n = 3 independent experiments). **d-e)** Gene expression levels as in **a-c** for MDA-MB-231 and PDC-BRC-101 cell lines treated with DOC following the treatment scheme shown in **Fig. 2i**., displayed as fold change (to DOC) of 2^{-dCt} values (relative to HK-genes). Unpaired t-tests based on relative expression values (2^{-dCt}) (n = 3 independent experiments). Data are presented as Mean ± SEM. **f-h)** Western blot analysis of Wnt ligand Wnt-2b in MDA-MB-231, MDA-MB-468, and PDC-BRC-101 cell lines treated with DOC or CAR for 72h. **i-k)** Western blot analysis of PORCN in TNBC cell lines treated with DOC or CAR for 72h. **l)** Schematic representation of Conditioned Media (CM) experimental setup. **m-n)** Flow Cytometry analysis displaying % of Wnt^{High} (GFP^{+}) cells of MDA-MB-231-TGP and MDA-MB-468-TGP cell lines cultured with concentrated Basal-, DOC-, or CAR-CM for 48h. Unpaired t-tests (n = 3 independent experiments). Data are presented as Mean ± SEM. **o)** Schematic representation of Co-culture experiment setup. **p)** Flow Cytometry analysis displaying % of Wnt^{High} (GFP^{+}) cells of chemo-naïve MDA-MB-231-TGP.mC co-cultured with chemo-treated DOC or CAR MDA-MB-231 cells for 72h. Unpaired t-tests (n = 3 independent experiments). Data are presented as Mean ± SEM. p values are indicated as *p < 0.05, **p < 0.01, ***p < 0.001, ****p < 0.0001, and ns, not significant.

FIG5

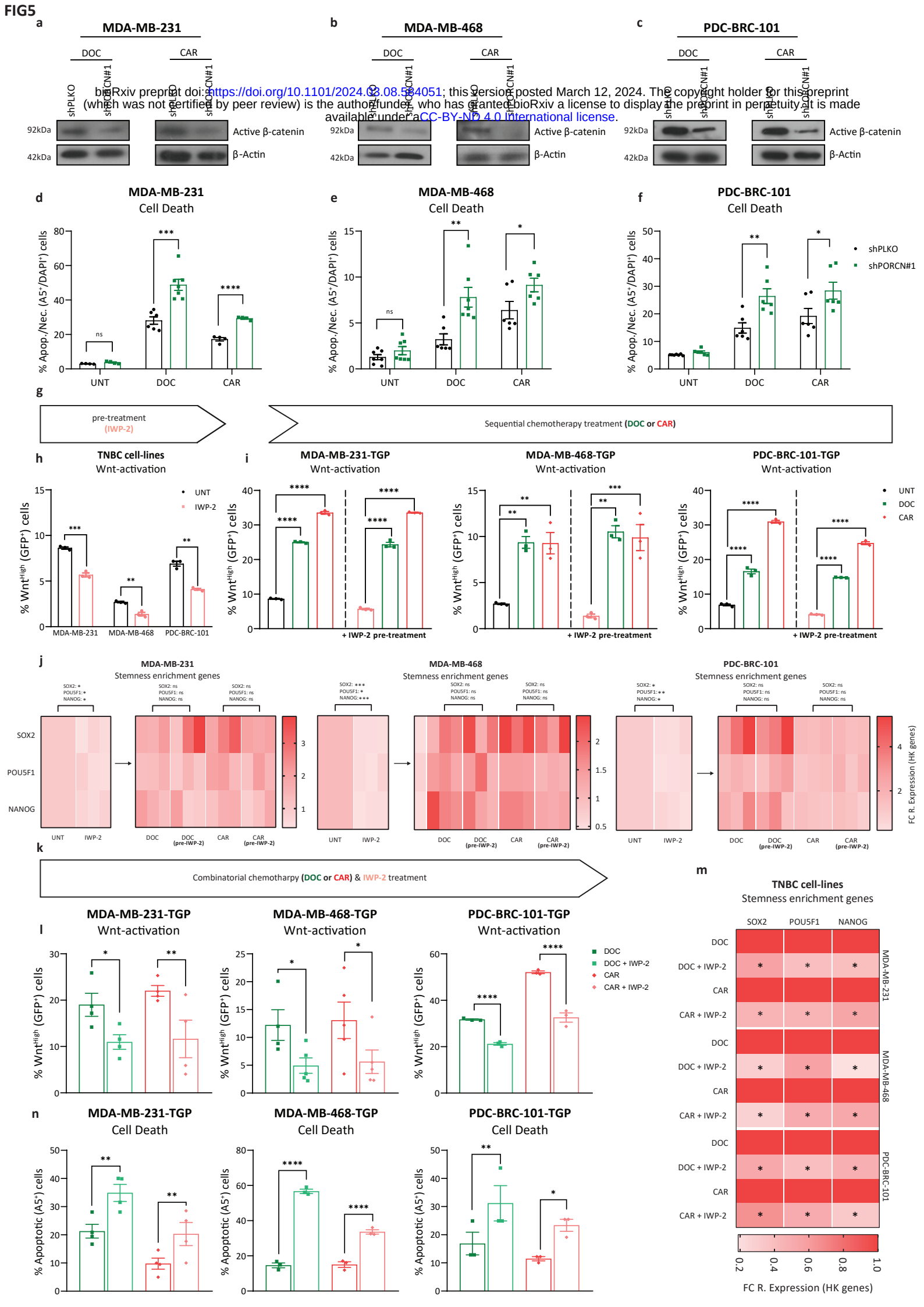

Figure 5: Concomitant inhibition of Wnt ligand secretion enhances chemotherapeutic sensitivity in TNBC

a-c) Western blot analysis of active- (non-phosphorylated) β-catenin in MDA-MB-231, MDA-MB-468, and PDC-BRC-101 (shPLKO vs. shPORCN#1) cell lines treated with DOC or CAR for 96h. **d-f)** Flow cytometry analysis displaying % Annexin V^+/$DAPI^+$ cells of MDA-MB-231, MDA-MB-468, and PDC-BRC-101 (shPLKO vs. shPORCN#1) cell lines treated with DOC or CAR for 96h. Unpaired t-tests (n = 4 independent experiments). Data are presented as Mean ± SEM. **g)** Schematic representation of the Sequential Treatment (first IWP-2 pre-treatment followed by chemotherapy) model. **h)** Flow cytometry analysis displaying % of Wnt^{High} (GFP^+) cells of MDA-MB-231-TGP, MDA-MB-468-TGP, and PDC-BRC-101-TGP cell lines pre-treated with IWP-2 (10uM) for 48h and treated with DOC or CAR for 72h (with or without IWP-2 pre-treatment). Multiple t-tests corrected for multiple comparisons using the Holm-Sidak method (n = 3 independent experiments). Data are presented as Mean ± SEM. **i)** Flow cytometry analysis of Wnt^{High} (GFP^+) cells of TNBC-TGP cell lines treated with DOC or CAR for 72h (with or without IWP-2 pre-treatment). Multiple t-tests corrected for multiple comparisons using the Holm-Sidak method (n = 3 independent experiments). Data are presented as Mean ± SEM. **j)** Heatmaps showing gene expression levels obtained via RT-qPCR of stem cell markers for TNBC cell lines treated with DOC or CAR for 72h (with or without IWP-2 pre-treatment), displayed as fold change (to UNT) of 2^{-dCt} values (relative to HK-genes). Multiple t-tests corrected for multiple comparisons using the Holms-Sidak method based on relative expression values (2^{-dCt}) (n = 3 independent experiments). **k)** Schematic representation of the Combinatorial Treatment model. **l)** Flow cytometry analysis displaying % of Wnt^{High} (GFP^+) cells of TNBC-TGP cell lines treated with DOC or CAR for 96h (sole or in combination with IWP-2). Unpaired t-tests (n = 4 independent experiments). Data are presented as Mean ± SEM. **m)** Heatmaps showing gene expression levels obtained via RT-qPCR of pluripotent stem cell markers for TNBC cell lines treated with DOC or CAR for 96h (sole or in combination with IWP-2), displayed as fold change (to sole treatment) of 2^{-dCt} values (relative to HK-genes). Unpaired t-tests between (DOC vs. DOC + IWP-2 and CAR vs. CAR + IWP-2, for every gene in every cell line) based on relative expression values (2^{-dCt}) (n = 3 independent experiments). **n)** Flow cytometry analysis displaying % of Annexin V^+ cells of TNBC cell lines treated with DOC or CAR for 96h (sole or in combination with IWP-2). Unpaired t-tests (n = 4 independent experiments). Data are presented as Mean ± SEM. p values are indicated as *p < 0.05, **p < 0.01, ***p < 0.001, ****p < 0.0001, and ns, not significant.

FIG6

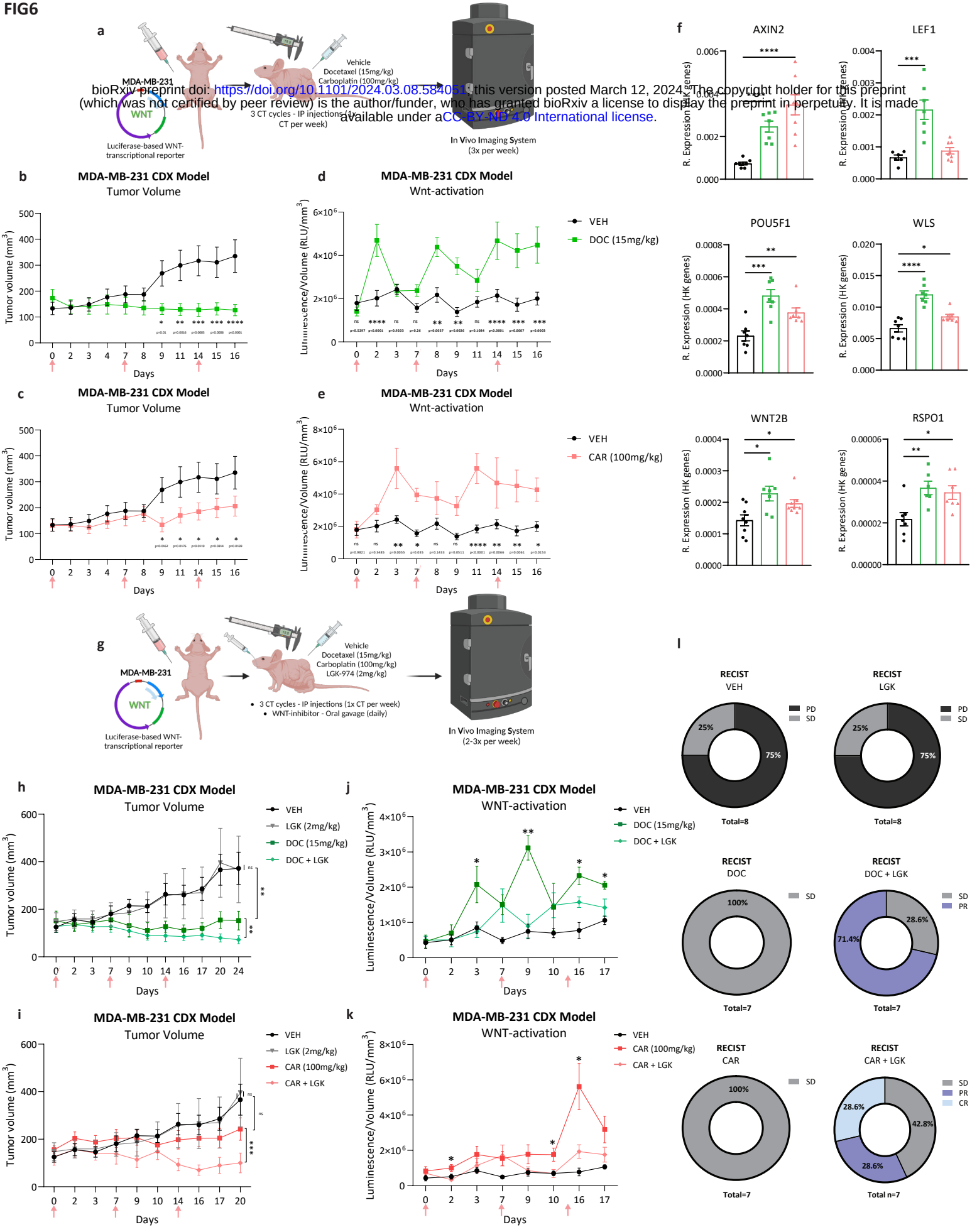

Figure 6: Inhibition of Wnt ligand secretion and chemotherapeutic treatment synergistically sensitize *in vivo* xenograft TNBC model to treatment

a) Schematic representation of cell line derived xenograft (CDX) experimental setup to study Wnt signaling pathway kinetics upon chemotherapeutic treatment *in vivo*. **b-c)** Tumor growth curves of subcutaneous generated xenograft models treated with VEH, DOC (15mg/kg/week – top), or CAR (100mg/kg/week – bottom). Pink arrows indicate administration of chemotherapy. Two-way ANOVA with Fisher's LSD test (n = 7 mice for all treatment groups). Data are presented as Mean ± SEM. **d-e)** Levels of Wnt-activation (RLU/mm³) displayed as luminescent signals (RLU) captured by IVIS Spectrum normalized to tumor volume (mm³) in xenograft models treated with VEH, DOC (top), or CAR (bottom). Two-way ANOVA with Fisher's LSD test (n = 7 mice for all treatment groups). Data are presented as Mean ± SEM. **f)** Gene expression levels obtained via RT-qPCR of various Wnt targets, stem cell markers, and Wnt-activators in samples resected from xenograft models treated with VEH, DOC, or CAR. Unpaired t-tests based on relative expression values ($2^{-\Delta ct}$) (n = 7 mice for all treatment groups). Data are presented as Mean ± SEM. **g)** Schematic representation of CDX experimental setup with Wnt ligand secretion inhibition *in vivo*. **h-i)** Tumor growth curves of xenograft models treated with VEH, LGK (2mg/kg/day), DOC (top), DOC+LGK (top), CAR (bottom), and CAR+LGK (bottom). Pink arrows indicate administration of chemotherapy. Paired t-tests (based on final tumor volumes – obtained on day of sacrifice, n = 8,7,6,5 mice per treatment group). Data are presented as Mean ± SEM. **j-k)** Levels of Wnt-activation (RLU/mm³) displayed as luminescent signals (RLU) captured by IVIS Spectrum normalized to tumor volume (mm³) in xenograft models treated with VEH, DOC (top), DOC+LGK (top), CAR (bottom), and CAR+LGK (bottom). Multiple t-tests (n = 8,7,6,5 mice per treatment group). Data are presented as Mean ± SEM. **l)** RECIST analysis displayed as percentage of animals per treatment group (VEH, LGK, DOC, DOC+LGK, CAR, and CAR+LGK) classified/assigned to one of four distinct tumor responses to treatment: Progressive Disease (PD), Stable Disease (SD), Partial Response (PR), or Complete Response (CR). p values are indicated as *p < 0.05, **p < 0.01, ***p < 0.001, ****p < 0.0001, and ns, not significant.

FIG7

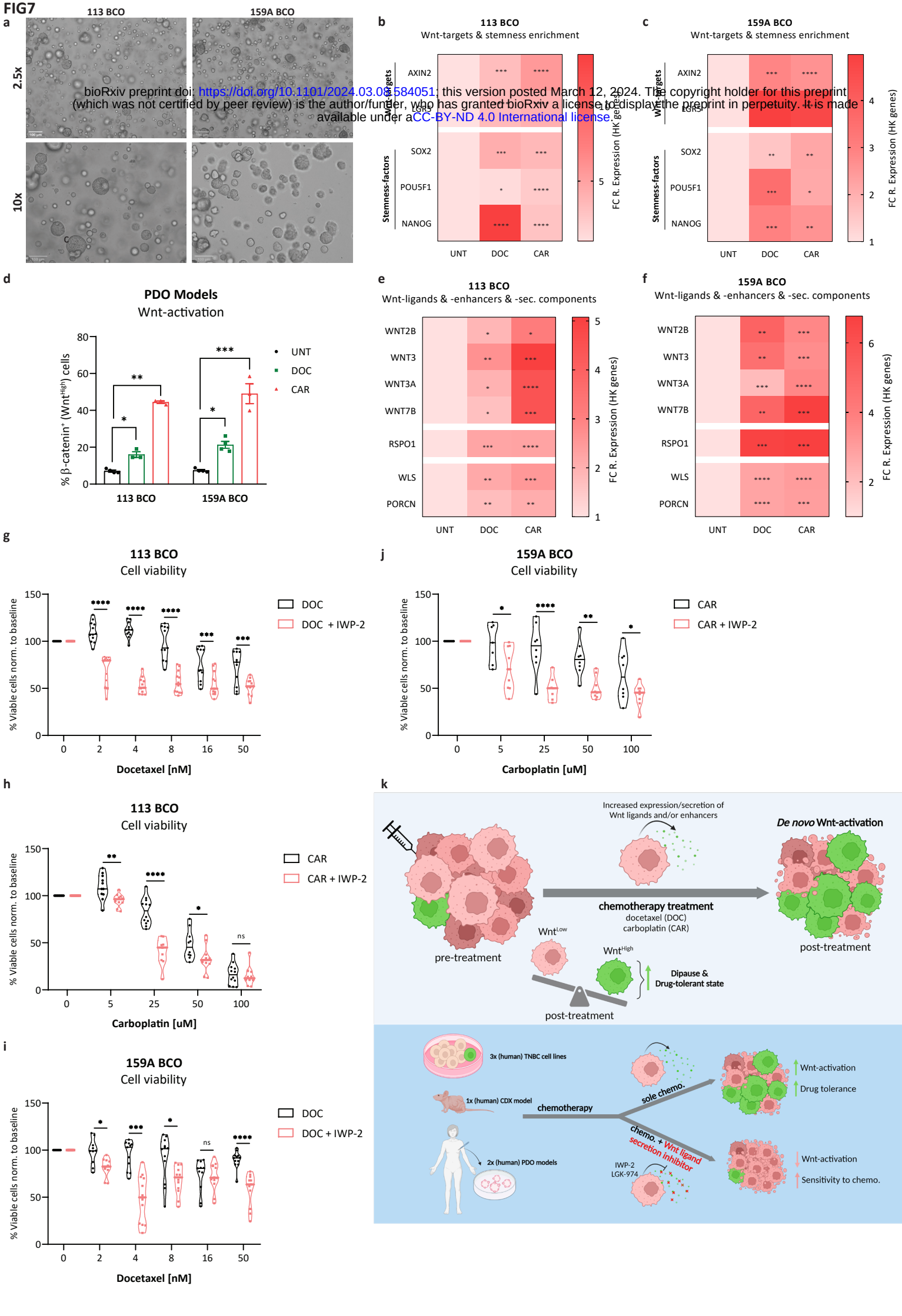

Figure 7: Preclinical PDO models recapitulate chemotherapy-mediated Wnt-activation and sensitization to synergistic Wnt ligand secretion inhibition

a) Phase-contrast images of TNBC-PDO models, 113 BCO (left) and 159A BCO (right) in basal culture conditions at 2.5x (top) and 10x (bottom) magnification **b-c)** Heatmaps showing gene expression levels obtained via RT-qPCR of Wnt-targets and stem cell markers for 113 BCO and 159A BCO models treated with DOC (16nM for 113 BCO and 8nM for 159A BCO) or CAR (50μM for 113 BCO and 125μM for 159A BCO) for 96h, displayed as fold change (to UNT) of 2^{-dCt} values (relative to HK-genes). Unpaired t-tests based on relative expression values (2dCt) (n = 4 independent experiments). **d)** Flow cytometry analysis displaying % of Wnt-active (β-catenin$^+$) cells from 113 BCO (left) and 159A BCO (right) models treated with DOC or CAR for 96h. Multiple t-tests corrected for multiple comparisons using the Holm-Sidak method (n = 3 independent experiments). Data are presented as Mean ± SEM. **e-f)** Heatmaps showing gene expression levels obtained via RT-qPCR of Wnt ligands, enhancers, and secretion machinery components for 113 BCO (left) and 159A BCO (right) models treated with DOC or CAR for 96h, displayed as fold change (to UNT) of 2^{-dCt} values (relative to HK-genes). Unpaired t-tests based on relative expression values (2^{-dCt}) (n = 4 independent experiments). **g-j)** Drug dose-response curves of 113 BCO (left) and 159A BCO (right) models treated with increasing concentrations of DOC or CAR (sole or in combination with IWP-2, 50uM). Viability in sole- or combinatorial-treatment is normalized to UNT or sole-IWP-2 conditions (baseline). Multiple t-tests corrected for multiple comparisons using the Holm-Sidak method (n = 4 independent experiments). Data are presented as Mean ± SEM. **k)** Graphical illustration representing a schematic summary of key findings and observations. p values are indicated as *p < 0.05, **p < 0.01, ***p < 0.001, ****p < 0.0001, and ns, not significant.